metals

MDPI

Review

Microstructural Characteristics and Strengthening Mechanisms of Ferritic–Martensitic Dual-Phase Steels: A Review

Farzad Badkoobeh [1,2,*], Hossein Mostaan [2,*], Mahdi Rafiei [3], Hamid Reza Bakhsheshi-Rad [3] and Filippo Berto [4,*]

[1] School of Metallurgy and Materials Engineering, College of Engineering, University of Tehran, Tehran, Iran
[2] Department of Metallurgy and Materials Engineering, Faculty of Engineering, Arak University, Arak, Iran
[3] Advanced Materials Research Center, Department of Materials Engineering, Najafabad Branch, Islamic Azad University, Najafabad, Iran; m.rafiei@pmt.iaun.ac.ir (M.R.); rezabakhsheshi@pmt.iaun.ac.ir (H.R.B.-R.)
[4] Department of Mechanical and Industrial Engineering, Norwegian University of Science and Technology, 7491 Trondheim, Norway
* Correspondence: farzad.badkoobeh@ut.ac.ir (F.B.); h-mostaan@araku.ac.ir (H.M.); filippo.berto@ntnu.no (F.B.)

Abstract: Ferritic–martensitic dual-phase (DP) steels are prominent and advanced high-strength steels (AHSS) broadly employed in automotive industries. Hence, extensive study is conducted regarding the relationship between the microstructure and mechanical properties of DP steels due to the high importance of DP steels in these industries. In this respect, this paper was aimed at reviewing the microstructural characteristics and strengthening mechanisms of DP steels. This review article represents that the main microstructural characteristics of DP steels include the ferrite grain size (FGS), martensite volume fraction (MVF), and martensite morphology (MM), which play a key role in the strengthening mechanisms and mechanical properties. In other words, these can act as strengthening factors, which were separately considered in this paper. Thus, the properties of DP steels are intensely governed by focusing on these characteristics (i.e., FGS, MVF, and MM). This review article addressed the improvement techniques of strengthening mechanisms and the effects of hardening factors on mechanical properties. The relevant techniques were also made up of several processing routes, e.g., thermal cycling, cold rolling, hot rolling, etc., that could make a great strength–ductility balance. Lastly, this review paper could provide substantial assistance to researchers and automotive engineers for DP steel manufacturing with excellent properties. Hence, researchers and automotive engineers are also able to design automobiles using DP steels that possess the lowest fuel consumption and prevent accidents that result from premature mechanical failures.

Keywords: advanced high strength steels; dual-phase steels; microstructure; strengthening mechanisms; mechanical properties; strength–ductility balance

Citation: Badkoobeh, F.; Mostaan, H.; Rafiei, M.; Bakhsheshi-Rad, H.R.; Berto, F. Microstructural Characteristics and Strengthening Mechanisms of Ferritic–Martensitic Dual-Phase Steels: A Review. *Metals* **2022**, *12*, 101. https://doi.org/10.3390/met12010101

Academic Editors: Andrea Di Schino and Roumen Petrov

Received: 2 November 2021
Accepted: 23 December 2021
Published: 5 January 2022

1. Introduction

Nowadays, famous steels referred to as advanced high-strength steel (AHSS) are highly regarded [1–7]. These steels have a superior balance of strength and ductility, resulting in the broad application of these steels in automotive industries [8–11]. The weight of automobiles made using these steels is dramatically reduced; thus, fuel consumption can be minimized [12–17]. According to Figure 1, AHSSs are categorized into three important groups: first generation, second generation, and third generation [8]. The members of the first generation are composed of dual-phase (DP) steels, complex phase (CP) steels, transformation-induced plasticity (TRIP) steels, and martensitic (MART) steels, while second-generation members are composed of austenitic stainless steels, lightweight steels with induced plasticity (L-IP), and twinning-induced plasticity (TWIP) steels, and finally, third-generation members are composed of medium manganese (Mn) TRIP steels, quenching and partitioning (Q&P) steels, and carbide-free bainitic (CFB) steels [8].

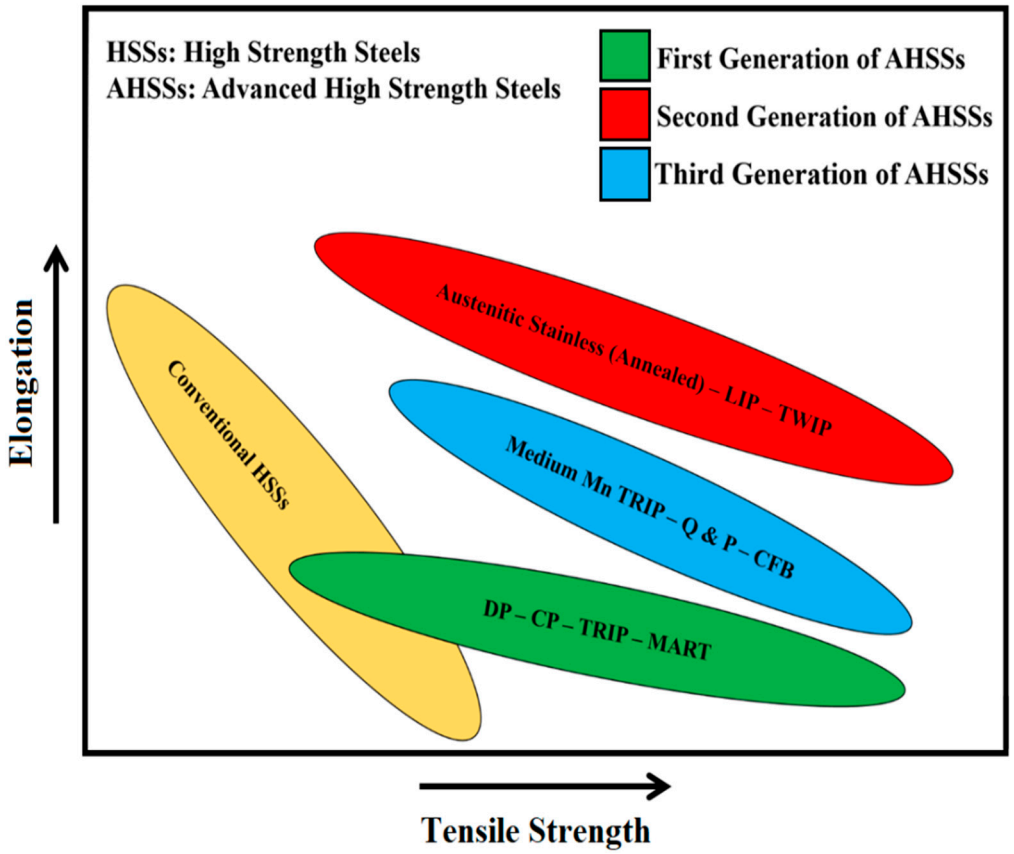

Figure 1. Relative and qualitative comparison of the strength–ductility balance of AHSSs versus other conventional high-strength steels Reprinted with permission from ref. [8]. Copyright 2021 Elsevier.

One of the well-known and outstanding members of AHSSs is DP steel [8,12,18–20]. Although DP steels are placed in the first generation of AHSSs, as shown in Figure 1 [8], extensive research is still being conducted regarding AHSSs [21–25]. The behavior of DP steels has exhibited that these steels are significantly competitive with newer generations of AHSSs (i.e., second and third generation) [1,2,13,26]. The microstructure of DP steels consists of the ferrite phase (matrix) and martensite phase (islands dispersed in the matrix) [27–29]. Accordingly, these steels can also be considered as a composite [13,30–32]; hence, the ferrite and martensite phases play the role of matrix and reinforcement, respectively [13,30,33,34]. In DP steels, similar to composites, the interface between these two phases is also important and strongly affects the properties of the steel. Due to the presence of high dislocation density within ferrite close to the interface of the ferrite/martensite and a deformation incompatibility between ferrite and martensite, there is great attention to the deformation behavior of DP steel [35–37]. Due to the microstructure, desirable mechanical properties such as high strength, appropriate ductility, good formability, high strain hardening rate, great strength–ductility balance, high crash resistance, very good fracture toughness, and excellent weldability are obtained [13,38–46]. The microstructural characteristics affect the behavior of ferritic–martensitic DP steels, such as mechanical performance, bake hardenability, weldability, corrosion, and wear properties [12,41,47–51]. The main microstructural characteristics of these steels are ferrite grain size (FGS), martensite volume fraction (MVF), and martensite morphology (MM). The range of strength and ductility of DP steels can be extended as compared to other generations of AHSSs via the change of these microstructural characteristics [12,30,52]. Accordingly, high strength and excellent ductility can be maintained simultaneously. Consequently, lower thicknesses of DP steels can be utilized to manufacture automotive components, which will have a remarkable effect on the automotive's weight loss and therefore fuel consumption [38,53,54]. In DP steel, the microstructural characteristics can be focused on to improve the strength [12,30,52].

It is worth noting that texture formation in DP steels is an important issue due to impressing formability that should be considered [4,5,51]. Yuan et al. [5] worked on the effect of temperature of warm rolling on the texture in DP steels. Their result exhibited that a predominant γ-fiber and a weak α-texture were developed in ferrite during warm rolling [5]. Moreover, during annealing of the rolled steel, the intensity of γ-fiber was enhanced and a weak texture of {001}<100> was developed in the rolled steel at room temperature [5]. In this respect, their result depicted that the strength of the undesirable texture of {001}<110> in the annealed steel firstly decreased and subsequently increased by enhancing the rolling temperature [5]. Furthermore, the strength could attain a maximum level at a rolling temperature of 550 °C by enhancement of the carbon dissolved in the ferrite arising from the carbide dissolution [5]. However, the intensity of the γ-fiber continued to be relatively greater when it was supposed to be the weaker {001}<110> component in the annealed steel rolled at a temperature of 450 °C [5]. Consequently, they described that a higher texture factor (i.e., $\frac{f_{\gamma-fiber}}{f_{(\alpha-fiber+\lambda-fiber)}}$) is predominant under this process [5]. Khosravani et al. [51] evaluated the texture of bake-hardened DP steels. Their result revealed that all ferrite textures illustrate the components of α-fiber, β-fiber, and a cube [51]. In addition, the strongest texture component could change from the component of {001}110 α-fiber to the component of {111}110 β-fiber through performing cold working [51]. However, the differences in texture between steels were less significant [51]. Kalashami et al. [4] demonstrated that an increment of niobium content led to an increase in the intensity of the components of {111} fiber, which is beneficial to the drawability of DP steels [4]. This review article eventually presents the microstructural characteristics of DP steels, the strengthening induced by them (i.e., FGS, MVF, and MM characteristics), the improvement techniques of hardening mechanisms, and their relationship with the mechanical behavior in DP steels.

2. Microstructural Characteristics of DP Steels

In DP steels, there are two phases of ferrite and martensite. The ferrite is the matrix, and the martensite phase is formed as a secondary phase inside the ferrite matrix, as shown in Figure 2. These two phases make key microstructural characteristics of FGS, MVF, and MM. Transmission electron microscopy (TEM) and electron backscatter diffraction (EBSD) studies have proven that there are a high number of dislocations inside the ferrite matrix close to the ferrite/martensite interface [55–59]. These dislocations are called geometrically necessary dislocations (GNDs). Based on Figure 2a,b, GNDs can be observed in the mentioned region [55,60]. Concerning Figure 2c,d, the lowest kernel average misorientation (KAM) belongs to the ferrite phase, marked by blue color. While the highest KAM belongs to the martensite regions, as marked by red color [58,61]. Figure 2c,d also indicate that the amount of misorientation/orientation gradient is high in the ferrite adjacent to the ferrite/martensite interface as compared with other regions that confirm the presence of GNDs in this region with large KAM [58,61]. It should be noted that these GNDs are mobile and play a key role when combined with residual stresses obtained by martensitic transformation for the behavior of yielding and initial flow [58]. It has been found that the reason for the continuous yielding behavior of DP steels refers to the presence of moving dislocations within the ferrite phase caused by the transformation of austenite to martensite [58]. Meanwhile, a fraction of the retained austenite in the microstructure depends on the steel's heat treatment conditions (e.g., quenching temperature and quenching medium) and chemical composition, as seen in Figure 2e,f [62]. Because the retained austenite is unstable, the mechanical properties can be affected when its fraction is noticeable [63]. The retained austenite is transformed to martensite, similar to TRIP steels during tensile loading [8,64].

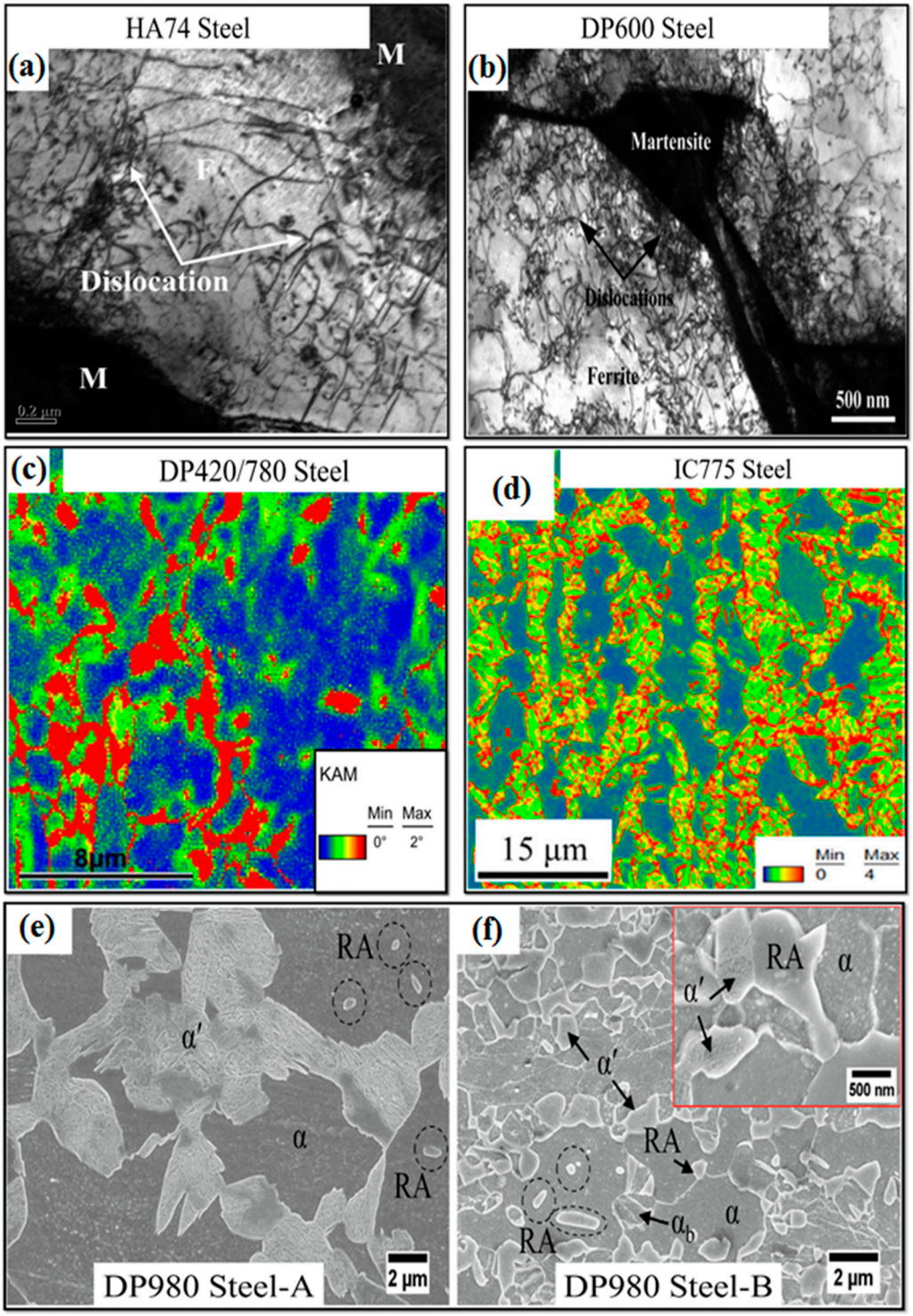

Figure 2. TEM image of DP steels: (**a**) HA74 steel [55] and (**b**) DP600 steel [60] (F = ferrite and M = martensite); KAM map of DP steels: (**c**) DP420/780 steel [58] and (**d**) IC775 steel [61]; SEM micrograph of DP steels: (**e**) DP980 steel–A and (**f**) DP980 steel–B [62]. Note: α = ferrite, α′ = martensite, α_b = bainite, and RA = retained austenite. Reprinted with permission from refs. [55,58,60,62]. Copyright 2021 Elsevier.

Another microstructural characteristic of DP steels is related to the presence of twins, as displayed in Figure 3 [65,66]. There are twins inside the martensite adjacent to ferrite, resulting from the shear deformation of austenite with a high shear strain rate. These are shown in Figure 3a–d [65,66]. Figure 3d corresponds to the selected area electron diffraction

(SAED) pattern of Figure 3c, which confirms the existence of twins within martensite [66]. Twins can also be formed in the ferrite/martensite interface and develop into ferrite where there is a high dislocation density [67]. The deformation twins in the body-centered cubic (BCC) structure are formed at low temperatures or high strain rates [67,68]. The velocity of austenite to martensite transformation is so high and is accompanied by high volumetric expansion. The strain rate that austenite endures during this transformation is very great as well [67]. Hence, it is anticipated that the ferrite phase also tolerates a very high strain rate via martensitic transformation and accommodates strain resulting from it through the deformation twins instead of dislocations sliding [67]. The relationship between the mean velocity of dislocations movement v and applied shear stress on the slip systems for deformation via dislocations sliding is determined according to Equation (1) [67,68]:

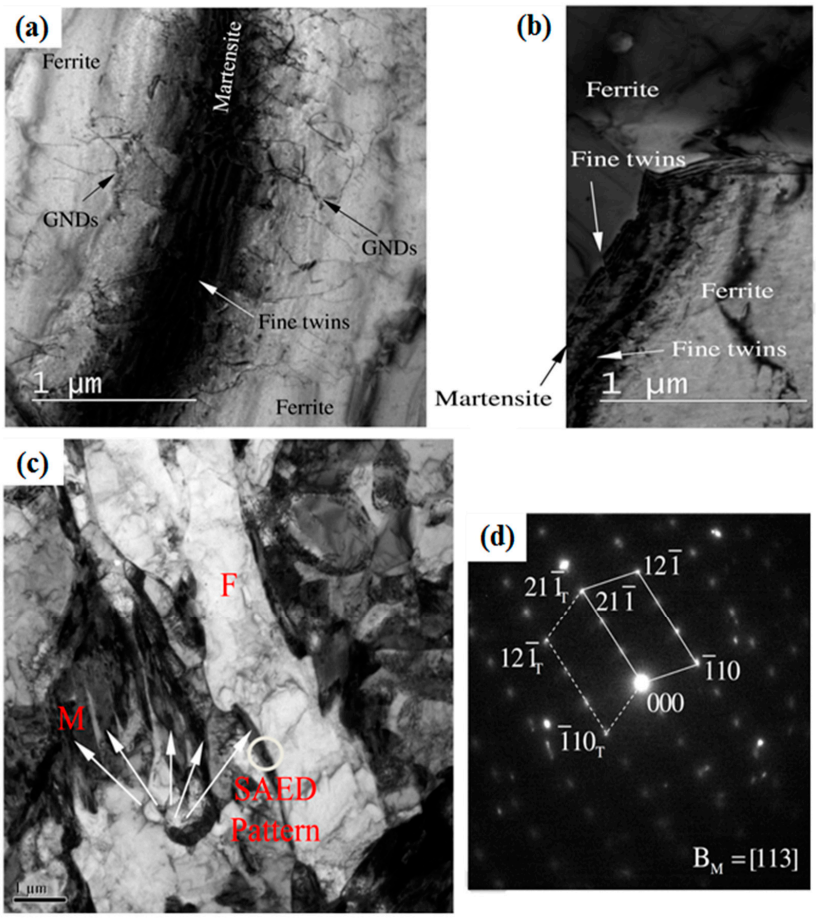

Figure 3. TEM micrographs of (**a**,**b**) DP steel [65], (**c**) DP steel (IQ steel), and (**d**) SAED pattern of (**c**) section. F = ferrite and M = martensite [66]. Reprinted with permission from refs. [65,66]. Copyright 2021 Elsevier.

$$v = (\tau/\tau_0)^m \quad (1)$$

where τ_0 and m are constants. Moreover, the correlation of the strain rate and mean velocity of dislocations movement is based on Equation (2) [67,68]:

$$\dot{\gamma} = \rho_m b v \quad (2)$$

where $\dot{\gamma}$, ρ_m, and b belong to the shear strain rate, the density of mobile dislocations, and the Burgers vector of dislocation, respectively. Equation (3) can be driven by the combination of Equations (1) and (2) [67,68]:

$$\dot{\gamma} = \rho_m b(\tau/\tau_0)^m \quad (3)$$

Equation (3) describes that a high density of mobile dislocations or high shear stress can cause a high strain rate. There is a low density of mobile dislocations inside the ferrite phase before the austenite to martensite transformation [67]. Accordingly, the ferrite phase cannot accommodate this high strain rate, owing to martensitic transformation via dislocations sliding, providing the deformation through the twins. Consequently, the twins can be formed within the ferrite [67].

3. The Strengthening Mechanisms of the DP Steels

The strengthening mechanisms in the materials are different. These mechanisms can result from strain hardening, grain refinement (grain boundaries), work hardening, solid solution, precipitation hardening, martensitic transformation, formation of strong texture, and interactions of the point defects with dislocations [68,69]. In DP steels, regarding their microstructural characteristics (Figure 2), four strengthening mechanisms of strain hardening, grain refinement, martensitic, and solid solution can be considered [1,42,43,47,52]. In addition, MM characteristics significantly affect the strengthening of DP steels [42,52,70]. It is evident that two phases of ferrite and austenite in the intercritical zone ($\alpha + \gamma$) were formed for producing DP steels at first [71]. Then, the austenite phase was transformed to the martensite phase via quenching [1,38,72]. The ferrite phase experiences a plastic strain with the occurrence of the martensitic transformation. Martensitic transformation is accompanied by an increase in volume, and a remarkable volumetric expansion takes place [35,73]. Therefore, the ferrite phase that is around the austenite phase is subjected to the plastic strain produced by martensitic transformation. Consequently, a high density of dislocations is generated in the ferrite phase close to the ferrite/martensitic interface [35,73]. This expresses a strengthening caused by the strain hardening in ferrite. Equation (4) declares the correlation of strain induced by austenite to martensite transformation (i.e., martensitic transformation) with relevant volume increment/volumetric expansion [35]:

$$\varepsilon_{A\to M} = \begin{pmatrix} \delta/3 & 0 & 0 \\ 0 & \delta/3 & 0 \\ 0 & 0 & \delta/3 \end{pmatrix} \quad (4)$$

where $\varepsilon_{A\to M}$ and δ are the plastic strain generated by the transformation of austenite to martensite and volumetric expansion (or volume enhancement) corresponding to the martensitic transformation, respectively. Equation (4) verifies that an increase in volumetric expansion caused by the martensite formation increases the relevant plastic strain generated, causing an increase in the plastic strain experienced by the ferrite phase [35]. The density of the generated GNDs was calculated via EBSD using Equation (5) [58,73]:

$$\rho_{\mathrm{GND}} = 2\vartheta/ub \quad (5)$$

where ρ_{GND}, u, and b are the density of GNDs, misorientation angle, the unit length, and the magnitude of the Burgers vector, respectively. ϑ is determined by KAM values related to EBSD data. ϑ is also influenced by the volumetric expansion corresponding to the transformation of austenite to martensite. In other words, the strain generated by martensitic transformation, based on Equation (6) [35,58,73]:

$$\vartheta \propto \varepsilon_{A\to M} \propto \delta \quad (6)$$

It is known that ϑ increases by an increase in δ and $\varepsilon_{A\to M}$ in Equation (6). So, according to Equation (5), ρ_{GND} will increase. The density of the ferrite grain boundaries and the number of the source of dislocations are increased via the reduction of FGS, i.e., ferrite grain refinement [48,53,74–76]. Another important point is that a decrease in FGS affects the density and area of the ferrite/martensite interface [48,53,74–76]. Moreover, the total strain experienced by the ferrite phase during the transformation of austenite to martensite and the density of produced dislocations within it will be affected by this

area [35,48,73]. This describes the strengthening of DP steel as a result of FGS reduction. On the other hand, the martensite phase will be formed by the occurrence of martensitic transformation. Concerning Equation (7), this hard phase is made up of several strengthening mechanisms [69]: a supersaturated solid solution caused by the dissolution of carbon in the structure of the body-centered tetragonal (BCT), grain refinement due to a high density of boundaries of twins, packets and blocks, and strain hardening caused by a high density of dislocations [69]:

$$\sigma_y = \sigma_i + K\sqrt{c} + K_y d^{-1/2} + \alpha G b\sqrt{\rho} \quad (7)$$

where σ_y, σ_i, K, c, K_y, d, α, G, b, and ρ are the yield strength, the lattice resistance to the dislocations movement, constant, the concentration of dissolved atom, the locking parameter, the packet size, constant, shear modulus, the Burgers vector, and dislocations density, respectively. It should be noted that the concentration of the solute carbon in the martensite phase plays a dominant role in the hardness and strength of this phase [12,73]. As mentioned earlier, this issue illustrates the strengthening related to the martensitic structure [38,65,69], where the MVF significantly contributes to the strengthening of DP steel [77–79]. This can be attributed to the density and area of the ferrite/martensite interface, the level of strain applied to ferrite during the transformation of austenite to martensite, the density of dislocations created inside the ferrite, and the concentration of carbon dissolved in the martensite [13,38,58,80]. This implies that an increase in MVF has a significant role in strengthening DP steel. The MM is another factor that has a considerable effect on the strengthening of DP steel. The martensite phase can have various morphologies that the interface area between them and the ferrite phase is completely different [42,52,66,81]. Consequently, different plastic strains are applied to ferrite during martensitic transformation, and there will naturally be various densities of dislocations within it [42,52,66,81,82]. This represents the strengthening of DP steel in connection with MM. It is important to say that when the nucleation of austenite (i.e., martensite) begins and grows beside the ferrite phase, the ferrite grain boundaries are pinned through this. Therefore, austenite/martensite can immobilize the ferrite grain boundaries. This indicates the pinning effect of the ferrite grain boundaries induced by the formed martensite [12,13,38,83]. This behavior is expected since the secondary phase leads to such a phenomenon in composites and age-hardened alloys. The pinning effect of the ferrite grain boundaries will improve via an increase in the density and area of the ferrite/martensite interface [38,43,83]. In general, three key characteristics of FGS, MVF, and MM govern the mechanical properties of DP steels, since they play a prevailing role in the strengthening of DP steels [48,52,84]. It was confirmed that a relation can be proposed in which the final strength of DP steel is the sum of the contribution of each of these strengthening factors. This relation is in the form of Equation (8) [38,42,48,52,53]:

$$\Delta\sigma_{\text{DP Steel}} = \Delta\sigma_{\text{FGS}} + \Delta\sigma_{\text{MVF}} + \Delta\sigma_{\text{MM}} \quad (8)$$

where $\Delta\sigma_{\text{DP Steel}}$ is the final strength of DP steel. The terms $\Delta\sigma_{\text{FGS}}$, $\Delta\sigma_{\text{MVF}}$, and $\Delta\sigma_{\text{MM}}$ are also FGS, MVF, and MM strengthening, respectively. The contribution of corresponding terms to the strengthening factors varies depending on the condition of DP steel. Thus, these terms compete with each other and determine the final properties of DP steels. In one case, one strengthening factor may become dominant, and in another case, two or three strengthening factors may be activated simultaneously. These factors will be discussed in detail.

4. The Role of FGS, MVF, and MM on Strengthening of DP Steels

In this section, firstly, the contribution of the microstructural characteristics regarding the strengthening of DP steels is evaluated. Then, the promotion techniques of these mechanisms will be pointed out in detail. As discussed, FGS, MVF, and MM are the main microstructural characteristics of DP steels. These can develop independent strengthening factors such as FGS, MVF, and MM strengthening. It should be mentioned that in DP steels similar to the composites, the final strength is controlled by limiting the plastic deformation

of the matrix (i.e., ferrite) and increasing its strength through reinforcement (i.e., martensite) [30,38]. The strengthening mechanisms induced by microstructural characteristics are presented in the following sections.

4.1. FGS Contribution on the Strengthening

The ferrite phase plays the role of the matrix in DP steels [1]. Accordingly, FGS has a substantial impact on the strength of the matrix and DP steels [43]. The density and area of the ferrite grain boundaries increase via FGS reduction. Grain boundaries are operative obstacles to the movement and sliding of dislocations to stop and store them [48,68,69,85]. A decrease in FGS also increases the number of the source of dislocations [48,68,69]. On the one hand, a decrease in the FGS increases the density and area of the ferrite/martensite interface, which has two important effects: first, more total plastic strain via the occurrence of martensitic transformation is applied to the ferritic matrix, causing an increase in the density of dislocations produced within it close to the ferrite/martensite interface, concerning Equations (5) and (6) [35,43,48,76]. Hence, concerning Equation (9), it can be described that the area/density of the ferrite/martensite interface is directly proportional to the volumetric expansion and strain obtained by austenite to martensite transformation (i.e., martensitic transformation) [35]:

$$A_{F/M} \& \rho_{F/M} \propto \varepsilon_{A \to M} \propto \delta \tag{9}$$

where $A_{F/M}$ and $\rho_{F/M}$ are the interface area of ferrite/martensite and density of the ferrite/martensite interface, respectively. Second, the pinning effect of the ferrite grain boundaries is likely intensified [48,83]. On the other hand, a reduction of FGS decreases the mean free path of ferrite and the martensite size [42,48,73]. Furthermore, martensite distribution becomes more uniform [48]. As a result, reducing FGS makes a restriction in the plastic deformation of ferrite and its strength improves, resulting in an increase in the strength and strain hardening of DP steels [30,38,48]. Equation (10) expresses that the contribution of FGS strengthening is inversely proportional to FGS (d_F) [38,42,48,53]:

$$\Delta\sigma_{\mathrm{FGS}} \propto 1/d_F \tag{10}$$

The Equations (11) and (12) are also related to the effect of FGS on the strength of a DP steel. These equations confirm an increase in both yield strength (YS) and ultimate tensile strength (UTS), with a decrease in FGS value [35]. According to Equation (13), the renowned Hall–Petch relation is also an expression for improved strength via decreasing grain size (d) [68,69]:

$$\mathrm{YS\ (MPa)} = 406.99 + 3.98 \times d_{\alpha}^{-1/2} \tag{11}$$

$$\mathrm{UTS\ (MPa)} = 794.14 + 8.39 \times d_{\alpha}^{-1/2} \tag{12}$$

$$\sigma_y = \sigma_i + K_y \times d^{-1/2} \quad \text{(Hall–Petch relation)} \tag{13}$$

Moreover, Equations (14) and (15) declare that the dislocation density ρ possesses an inverse relationship with FGS and a direct relationship with the strength, respectively [68,69]:

$$\rho = 1/d_F \tag{14}$$

$$\sigma_y = \sigma_i + \alpha G b \sqrt{\rho} \tag{15}$$

Therefore, Equations (14) and (15) illustrate the increment of strength via FGS reduction. It was described that the back stresses applied by martensite islands and smaller FGS also contribute to the improvement of strain hardenability [48]. There are a variety of techniques to decrease FGS and improve the FGS role in the strengthening of DP steels. Several vital processing routes of reducing FGS will be noted to create fine-grained (FG) and ultrafine-grained (UFG) ferrite, which are presented in the following sections.

(1) The repetition of thermal cycling during intercritical annealing: In this processing route, intercritical annealing treatment is repeated as shown in Figure 4a. This leads to a reduction in FGS [86]. On the other hand, when DP steel includes a banded microstructure, the repetition of thermal cycling during intercritical annealing could modify the microstructure, so that this process will decrease the band spacing in addition to ferrite grain refinement. Such microstructural evolution is beneficial to the mechanical property [86]. It is worth noting that intercritical annealing treatment represents annealing at the $\alpha + \gamma$ region and then quenching to room temperature. They are further reduced by increasing the number of cycles. The mechanism of this processing route is related to the complex structure of martensite that has the laths (including the martensite crystals with a high density of lattice imperfections), the blocks (including a set of laths with similar crystallographic relationships), and the packets (including a set of blocks with similar habit planes), as seen in Figure 4b [3]. Approximately 83% of the boundaries of block and packet are a high angle [3,86–88]. Initially, the primary microstructure is ferritic–martensitic. Then, a finer ferrite in DP steel is formed by intercritical annealing treatment. During annealing, new austenite and ferrite grains are formed on the prior austenite grain boundaries (PAGB) and also on the boundaries of the packets and blocks. Because the density of nucleation sites is high, the nucleation rate also increases, and finer martensite and ferrite are formed. As a consequence, UFG ferrite can be achieved for DP steel through an increase in the number of cycles [86]. It is noted that, after a specific cycle, the formed martensite is fine enough. So, the new ferrite and austenite grains cannot be formed on the boundaries of the packet and block, and they are only created on the prior austenite grain boundaries. This means that grain refinement and reduced band spacing are saturated [86].

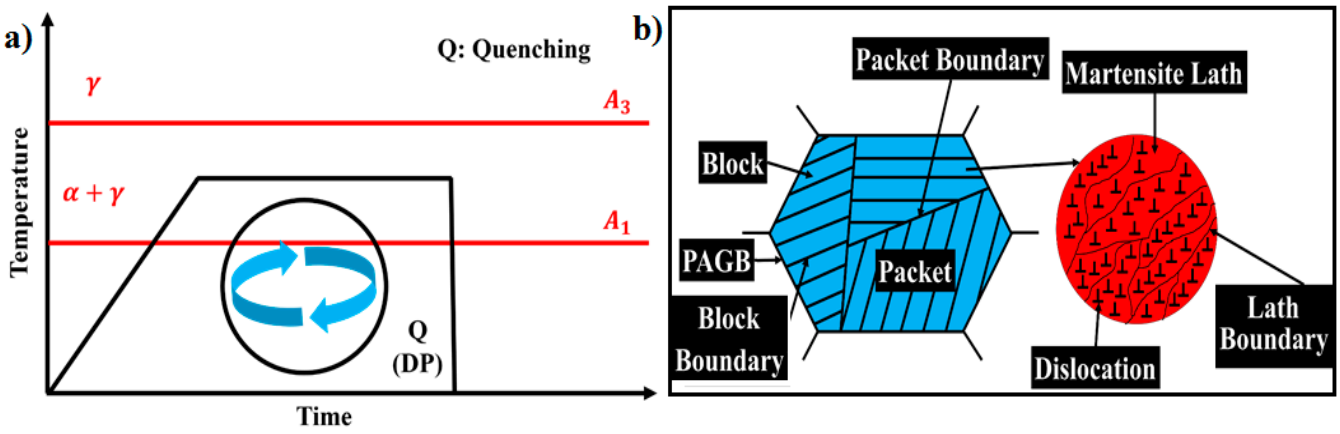

Figure 4. (**a**) Heat treatment regime (processing route 1) for FGS reduction. (**b**) The schematic structure of lath martensite phase. PAGB = prior austenite grain boundary [3]. Reprinted with permission from ref. [3]. Copyright 2021 Elsevier.

(2) Cold rolling of a martensitic steel, followed by intercritical annealing: In this processing route, the martensitic steel is cold rolled and then undergoes intercritical annealing treatment. As can be seen in Figure 5a, the steel microstructure is primarily quite martensitic, and cold rolling is performed. Then, UFG ferrite will be formed by intercritical annealing treatment. In fact, two mechanisms of grain subdivision and continuous recrystallization are considered [86]. The mechanism of grain subdivision can include the subdivision caused by martensitic transformation and the subdivision caused by the creation of dislocation cell blocks during the cold rolling. During annealing, dislocation cell blocks are transformed into UFG ferrite [86]. Nearly 83% of the block and packet boundaries are high angles, which are effective obstacles to the movement of the dislocations. On the other hand, martensite has supersaturated carbon, preventing their movement [86]. Accordingly, the formation of dislocation cells and cell blocks with a high density of dislocations is accelerated and facilitated during cold rolling. This describes the mechanism of

grain subdivision. Another mechanism that is activated during annealing is continuous recrystallization [86]. In this mechanism, at first, the lamellar structure of martensite collapses, which corresponds to the surface tension. Then, spheroidization occurs, which is associated with the boundary tension. Finally, spheroidization continues and grain growth may also occur [86]. This mechanism is shown in Figure 5b [85]. It is vital to note that nano-sized carbides also precipitate during annealing, which prevents grain growth. In this way, a DP steel with UFG ferrite is developed by intercritical annealing treatment after cold rolling [86].

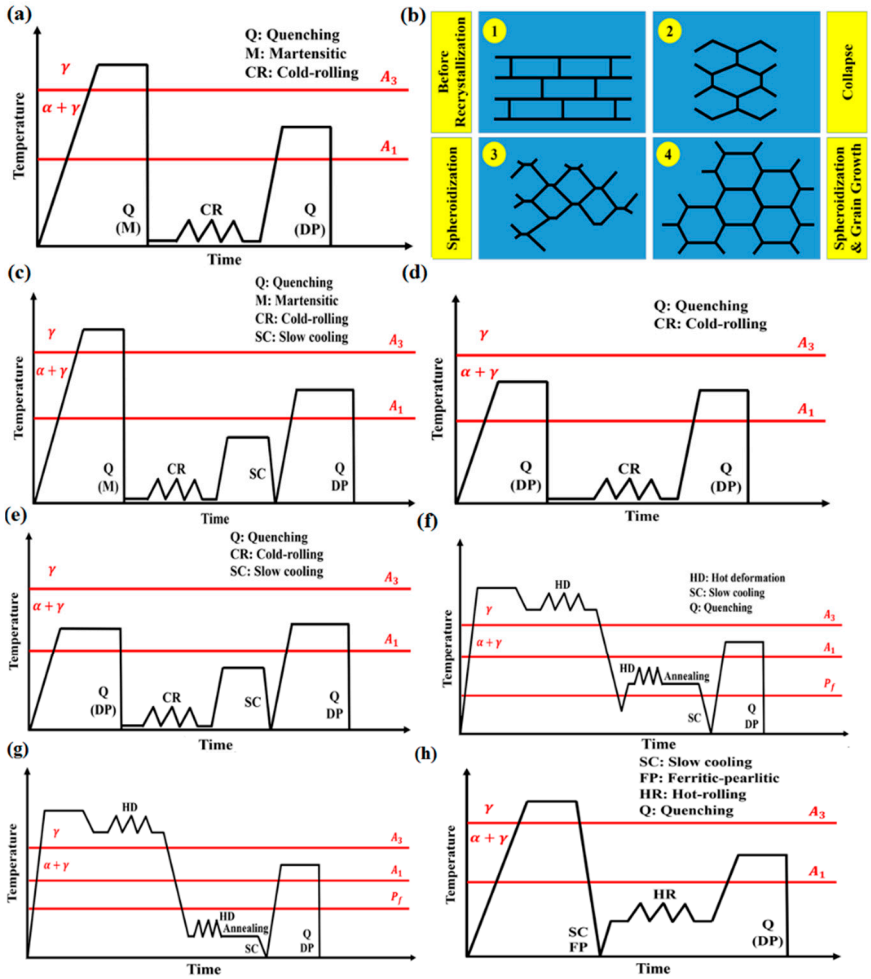

Figure 5. (**a**) The heat treatment regime (processing route 2) for FGS reduction. (**b**) Mechanism of continuous recrystallization: (1) before recrystallization, (2) collapse, (3) spheroidization, and (4) advancement of spheroidization and grain growth [85]. (**c**) Heat treatment regime (processing route 3). (**d**) Heat treatment regime (processing route 4). (**e**) Heat treatment regime (processing route 5). (**f**,**g**) Heat treatment regime (processing route 6). (**h**) Heat treatment regime (processing route 7) for FGS reduction. Reprinted with permission from ref. [85]. Copyright 2021 Elsevier.

(3) Cold rolling of a martensitic steel, followed by subcritical and intercritical annealing: In this process, after subcritical annealing of the cold-rolled martensitic steel below A_1 temperature, intercritical annealing treatment is applied. Concerning Figure 5c, firstly, the initial microstructure is quite martensitic. Then, cold rolling and subcritical annealing below A_1 temperature form a microstructure consisting of UFG ferrite, small tempered blocks of martensite, and nano-sized carbides based on the mechanisms discussed in processing route two [86]. These carbides are effective barriers to grain growth [86]. Eventually, a DP steel that includes UFG ferrite is developed by intercritical annealing treatment [86].

(4) Cold rolling of a DP steel, followed by intercritical annealing: As shown in Figure 5d, by cold rolling of a DP steel, both ferrite and martensite phases are elongated in the rolling direction, and a high density of dislocations is also generated. This provides the condition for recrystallization. It should be noted that the ferrite phase tolerates more plastic strain as compared to the martensite phase. This strain distribution between phases affects the final grain refinement [89–91]. The reason is that the martensite hard phase is at the vicinity of the soft ferrite phase, and the ferrite incurs the back stress from the martensite. This results in an increase in the stored energy in the ferrite during cold-rolling [89–91]. Generally, the remarkable plastic strain causes the deformation of both ferrite and martensite phases during the cold rolling. Accordingly, the deformed ferrite and martensite have an important role and contribution in grain refinement through ferrite recrystallization or reversion of martensite [89–91]. Finally, ferrite recrystallization takes place via intercritical annealing treatment, leading to the formation of UFG ferrite in DP steel [89–91].

(5) Cold rolling of a DP steel, followed by subcritical and intercritical annealing: In this cycle, cold-rolled DP steel undergoes subcritical annealing (below A_1 temperature) and then it experiences intercritical annealing treatment. This process is similar to processing route four until the cold-rolling stage of Figure 5e. By subcritical annealing, ferrite grain refinement occurs, which is due to the continuous recrystallization of martensite. Moreover, coarse-grained (CG) ferrite may be formed as a consequence of the primary recrystallization. Thus, a microstructure with bimodal distribution is achieved [92]. Finally, a DP steel with UFG ferrite is formed via intercritical annealing treatment [92].

(6) Hot deformation at the top and bottom of the pearlite final temperature (P_f): The steel is initially deformed *at the* γ *zone* and is then deformed at the top and bottom of P_f, as well as subsequent annealing at the relevant deformation temperature and slow cooling to the desired temperature, followed by intercritical annealing treatment. Based on Figure 5f, the microstructure will include fine polygonal ferrite with fine pearlite and globular cementite via hot deformation above P_f. However, concerning Figure 5g, through hot deformation below P_f, recovery and grain subdivision mechanisms cause the formation of the deformed ferrite grains. The lamellae of cementite in the pearlite colonies are fragmented and are spheroidized as well. Thus, a fine distribution of globular cementite is obtained in the ferrite grain boundaries. It is noted that after hot deformation, annealing is performed at the relevant deformation temperature [48]. Eventually, a DP steel will be developed, consisting of FG ferrite and UFG ferrite via intercrtical annealing treatment after the routes of Figure 5f,g, respectively.

(7) Hot rolling of a ferritic–pearlitic steel, followed by intercritical annealing: In this process, the steel is treated (hot-rolled) at a temperature below A_1 and then subjected to intercritical annealing treatment. Concerning Figure 5h, hot rolling leads to the formation of elongated ferrite and pearlite with intergranular nano-sized spheroidized carbides. These carbides can impede the ferrite grain growth. On the other hand, continuous recrystallization and grain subdivision can also occur. In this way, ferrite grains become smaller. Ferrite grain refinement improves with an increment in the rolling reduction, owing to an increased fraction of nano-sized carbides and a higher degree of continuous recrystallization and grain subdivision. It was also stated that the thickness of the ferrite layers decreases with an increase in the rolling reduction [93]. Thus, a DP steel with FG ferrite will be generated by intercritical annealing treatment. It seems that an increase in MVF is also effective on grain refinement with increasing rolling reduction [93].

(8) Primary hot rolling, followed by intercritical annealing as well as secondary hot rolling: In this heat-treatment cycle, the steel is treated (hot-rolled) at a temperature above A_3, then quenched to room temperature, followed by annealing at the $\alpha + \gamma$ zone and hot rolling along with quenching to room temperature. Regarding Figure 6a, martensite with a lamella structure is formed in step one. In step two, at first, ferrite and austenite are formed with layered morphology. Then, quenching is performed to a certain temperature below A_1, and UFG ferrite and lamella martensite are created through hot rolling at this temperature [30]. Finally, a DP steel including such a microstructure will be obtained by cooling to

room temperature [30]. In this processing route, the formed lamella martensite also induces a secondary strengthening mechanism that is caused by the MM characteristic [30].

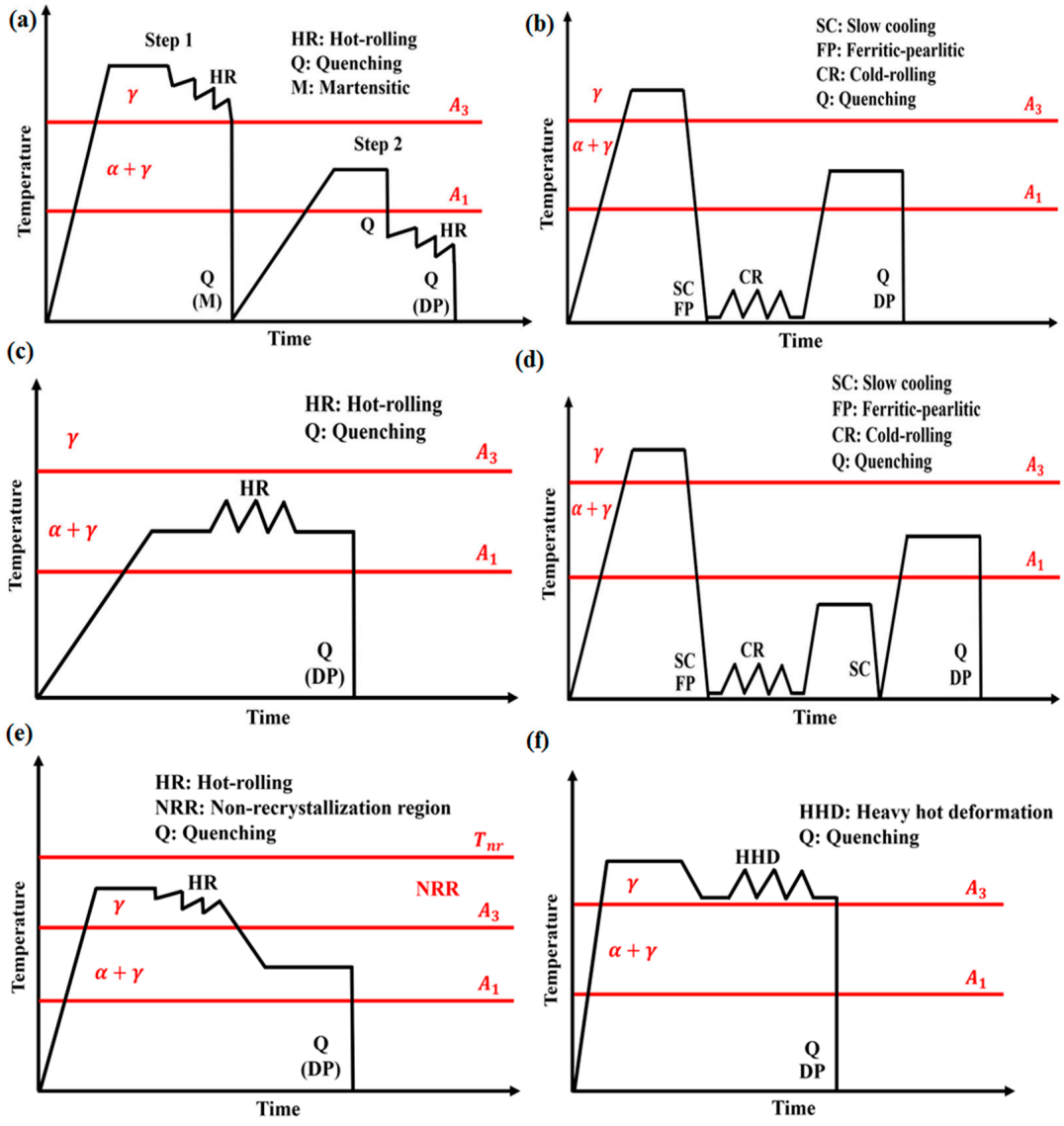

Figure 6. Various heat-treatment regimes: (**a**) processing route 8, (**b**) processing route 9, (**c**) processing route 10, (**d**) processing route 11, (**e**) processing route 12, and (**f**) processing route 13 for FGS reduction.

(9) Cold rolling of a ferritic–pearlitic steel, followed by intercritical annealing: The steel is cold rolled in this processing route and subsequently subjected to intercritical annealing treatment. According to Figure 6b, firstly, cold rolling causes the creation of elongated ferrite and pearlite in the rolling direction, providing the condition for ferrite recrystallization. Then, UFG ferrite in DP steel is formed by intercritical annealing treatment [94].

(10) Cold rolling of a ferritic–pearlitic steel, followed by subcritical and intercritical annealing: The steel is cold rolled in this heat-treatment cycle, experiences subcritical annealing below A_1 temperature, and undergoes intercritical annealing treatment. As observed in Figure 6c, initially, cold rolling causes the formation of a microstructure consisting of deformed ferrite and pearlite. Then, UFG ferrite and nanoscale cementite are created via subcritical annealing. The created UFG ferrite is due to recrystallization [38]. Ultimately, after intercritical annealing treatment, a DP steel including UFG ferrite is obtained [38].

(11) Hot rolling at the $\alpha + \gamma$ zone: The steel is hot rolled in this heat-treatment cycle at the intercritical zone of $\alpha + \gamma$ and then quenched in the desired medium. As illustrated in Figure 6d, hot rolling at the $\alpha + \gamma$ zone causes the formation of elongated austenite and ferrite. In this case, not only is the specific area of the grains corresponding to both phases enhanced, but a substructure is also developed within the ferrite. This process finally leads to a ferrite grain refinement that likely results from mechanisms such as grain subdivision and recrystallization [86,95]. After quenching, a DP steel consisting of FG or UFG ferrite will also be produced [86,95].

(12) Hot rolling at T_{nr} of austenite, followed by intercritical annealing: The steel is hot rolled in this heat-treatment cycle at the non-recrystallization temperature (T_{nr}) range of austenite and subsequently experiences intercritical annealing treatment. Thus, the austenite grains are elongated and pancaked as a result of hot rolling below T_{nr} of austenite, as shown in Figure 6e. Moreover, the specific area of grains is increased, and a deformed structure is created within them. This leads to a higher density of nucleation sites for ferrite and an acceleration of its nucleation rate inside the austenite and at the austenite grain boundaries [86]. Finally, with intercritical annealing treatment, a DP steel is developed with FG or UFG ferrite [86].

(13) Deformation-induced ferrite transformation (DIFT): This heat-treatment cycle corresponds to the changes in the distribution of dislocations, diffusion of the solute atoms, the occurrence of phase transformation, and the development of grain boundaries [96,97]. As seen in Figure 6f, a severe plastic deformation (SPD) close to A_3 temperature (roughly 25 to 100 °C above A_3) is accomplished to initiate DIFT. In this condition, phase transformation is more dominant than the austenite recrystallization resulting from favorable and feasible nucleation for ferrite via deformation. Noticeable undercooling below A_3 temperature causes an increment in the driving force for the ferrite nucleation and UFG ferrite is formed [96]. Deformation above A_3 temperature leads to an increase in the free energy and the transformation temperature of austenite to ferrite is also increaed. In this condition, austenite to ferrite transformation and ferrite nucleation are dynamically performed. This means that they occur during the austenite deformation, not after its deformation [96,97]. Heavy deformation results in increasing austenite free energy. Accordingly, the metastable austenite is converted into the unstable austenite and DIFT is complete [96]. The level of strain applied is so important. It was reported that a relatively high strain level is necessary for ferrite grain refinement. Most of the CG ferrite is converted into the FG ferrite, resulting from an increase in the density of nucleation sites for ferrite [96]. So, at low strain levels, the density of the nucleation sites is lower and CG ferrite is created [96]. Another key point is that changes in the prior austenite grain sizes also alter A_3 temperature, affecting the deformation temperature during DIFT [96]. Larger prior austenite grain sizes (produced by a high austenitization temperature) lead to a delay in ferrite formation. However, by its reduction, deformation-induced ferrite develops more uniformly in the austenite grains owing to deformation [96]. For this reason, more DIFT will be accomplished, resulting in finer austenite grains and more austenite grain boundaries [96]. Lastly, as DIFT is carried out, a DP steel with UFG ferrite is obtained through quenching [96].

(14) High heating rates during intercritical annealing treatment: It was confirmed that high heating rates during intercritical annealing treatment play a significant role in ferrite grain refinement [98]. High heating rates delay recovery and recrystallization processes, resulting in the annihilation of high stored energy, dislocations, and point imperfections. On the other hand, high heating rates accelerate the kinetics of ferrite recrystallization, austenite formation, and their spatial distribution and morphology [98]. Meanwhile, the enhanced heating rate increases the superheating. This causes an increase in the nucleation rate and the grain growth rate of the austenite in the $\alpha + \gamma$ zone simultaneously. However, it is noteworthy that the nucleation rate is greater than the grain growth rate, causing grain refinement [98]. At a low heating rate, firstly, as heating is performed in cold-rolled steel up to the $\alpha + \gamma$ zone, ferrite recrystallization is completed. Then, the austenite nucleation occurs in the grain boundaries of the recrystallized ferrite, and a network of

the austenitic phase, due to the grain growth of the austenite, is developed along the ferrite grain boundaries [98]. At a moderate heating rate, when the austenite nucleation starts, the volume fraction of non-recrystallized ferrite increases. Carbon atoms are also distributed along the grain boundaries of the deformed ferrite. Austenite nucleation occurs in carbon-rich regions, arising from the lower Gibbs free energy in them. Thus, austenite nucleation is mostly initiated in the grain boundaries of non-recrystallized ferrite. In this case, the austenite nucleation rate is higher than the ferrite nucleation rate, and a banded microstructure is developed in DP steel [98]. The banded microstructures in DP steels are detrimental to the mechanical properties [31,98]. Ramazani et al. [31] examined the correlation of martensite banding with the failure initiation in DP steel [31]. Their result exhibited that the major mechanism of the failure initiation is martensite cracking in the equiaxed and banded microstructures of DP steels [31]. They showed that the failure initiation could occur in the lower plastic strain for the banded microstructure as compared to the equiaxed microstructure [31]. Consequently, the banded microstructure in DP steels leads to a drop in the failure behavior, and its formation should be prevented. The equiaxed microstructure in DP steels causes the improved failure behavior [31]. At a high heating rate, the microstructure consists of completely deformed and non-recrystallized ferrite in the $\alpha + \gamma$ region. In this case, there are carbides distributed along the deformed ferrite grain boundaries, leading to an increase in the density of nucleation sites. This also accelerates the growth of austenite at a high sufficient annealing temperature until all deformed ferrite grain boundaries are concealed. Then, at the same time, ferrite recrystallization commences. Finally, ferrite grain refinement takes place [98]. The reason for this can be attributed to the overlap between the austenitization and the ferrite recrystallization processes during annealing [98]. In this way, a DP steel with FG or UFG ferrite is developed [98].

(15) Chemical composition: Chemical composition is one of the significant factors in grain refinement [95,99,100]. It has been confirmed that the silicon element can decrease and increase FGS [28,49]. Nouri et al. [49,50] expressed that increasing the silicon content increased FGS. This more likely resulted from decreasing MVF (this reason will be discussed) and increasing the mobility of ferrite grain boundaries [49,50]. Zhou et al. [28] showed that increasing the silicon content decreased FGS. This could be due to the enhancing nucleation rate of the ferrite phase and the increment of the carbon activity in austenite via increasing the silicon content caused by suppression of the carbide formation, leading to an increase in the driving force for the austenite to ferrite transformation [28]. Consequently, the addition of silicon can cause ferrite grain refinement [28]. Drumond et al. [100] also concluded with the same result. Their result depicted that the addition of silicon speeds up the ferrite recrystallization by producing a greater thermodynamic potential for it during intercritical annealing of cold-rolled steel [100]. Accordingly, silicon could refine FGS [100]. Other studies [2] revealed a refined microstructure via chromium addition. Moreover, carbide, nitride, and carbonitride-producing elements, e.g., niobium, titanium, zirconium, aluminum, molybdenum, nitrogen, and vanadium, can contribute to ferrite grain refinement [2,4,95,101]. Since the precipitations formed by these elements during intercritical annealing treatment result in the pinning of the grain boundaries, their mobility is decreased, which leads to refined FGS [2,95]. It is noted that these precipitations have a tendency to mostly create in the ferrite phase, caused by a greatly lower solubility of the carbides/nitrides in this phase in comparison with their solubility in the austenite phase [2]. Overall, microalloying elements can be very beneficial for this purpose [4,95,101]. It was reported that the addition of niobium in the form of solute atoms and precipitations decreases the mobility of dislocations. This is in connection with the solute drag mechanism. Therefore, the processes of recovery, recrystallization, and growth of the deformed austenite grains are postponed [95]. As a result, the driving force of austenite to ferrite transformation is promoted, and the ferrite nucleation is accelerated. Moreover, niobium can prevent grain growth at the $\alpha + \gamma$ region. Then, a DP steel including FG or UFG ferrite can be obtained with intercritical annealing [95]. It was revealed that the addition of manganese is also effective on the ferrite grain refinement in DP steel. This

can be attributed to the grain size stability that is caused by [102]: (a) the reduction of A_1 temperature and intercritical annealing temperature, (b) the extension of the triple-phase region of ferrite + austenite + cementite and retardation of the grain growth in this region, (c) refinement of cementite, leading to an increase in the pinning effect of grain boundaries, and (d) the mobility reduction of the grain boundaries as a result of the solute drag mechanism. These have a strong impact on the formation of UFG ferrite.

(16) Increment of MVF: Researchers state that increasing MVF can also play a role in ferrite grain refinement. Martensite as a secondary phase can lock the ferrite grain boundaries [38,53]. Hence, their mobility decreases, causing the suppression of ferrite grain growth and a decrease in FGS. In this way, good grain refinement of ferrite can be achieved with an increase in MVF [38,53]. In all the mentioned processing routes, parameters such as the rolling reduction, the strain rate, the rolling temperature, the annealing temperature, the annealing time, and the heating rate can affect grain refinement. Many SPD techniques, such as friction stir processing, accumulative roll bonding, equal channel angular pressing, could refine grains [75,85,97,103]. Their grain refinement mechanism is mainly related to dynamic recrystallization [75,85,97,103]. The presentation of these processing routes is not authors' aim. It was shown in a study that the reduction of FGS decreased the hardness and strength of DP steels [104]. As noted, the decrement of FGS increases the density of the ferrite/martensite interface, causing the generation of a high density of dislocations inside the ferrite [104]. Because these are moving and the distance between the regions of martensite is less, the yielding and the arrangement of dislocations for the achievement of necking occur in lower stresses [104]. Consequently, the hardness and strength will decrease [104]. Moreover, FGS decrement is beneficial for impacting the behavior of DP steels [43]. Equation (16) shows that the fracture appearance transition temperature (FATT) is reduced with grain size (D) decrement [86]:

$$\text{FATT} = A - B/\sqrt{D} \tag{16}$$

where A and B are constants. Moreover, the ductile-to-brittle transition temperature (DBTT) decreases with ferrite grain refinement, as illustrated by Calcagnotto et al. [43]. Accordingly, it is found that reducing FATT and DBTT finally causes an increase in fracture toughness and the impact energy of DP steel [43,86].

4.2. MVF Contribution on the Strengthening

Regarding the MVF effect on strengthening, it can be stated that the martensite phase acts as a reinforcement for the ferritic matrix [1,12,105]. So, MVF can control the strength of the matrix and DP steel [1,13,18,53]. An increment in MVF causes an increase in the density and area of the ferrite/martensite interface. Accordingly, the total plastic strain produced by the martensitic transformation will increase, leading to an increase in the strain tolerated by ferrite. Consequently, this increases the density of dislocations created within the ferrite adjacent to the ferrite/martensite interface, according to Equations (5), (6) and (9), and decreases the mean free path of ferrite [38,42,58,73]. Meanwhile, an increase in MVF locks more grain boundaries and improves the pinning effect of the ferrite grain boundaries [38,53,83]. Ultimately, it can be stated that an increase in MVF leads to an increase in the strength of matrix and DP steel [38,66,73]. Moreover, the strain hardenability of steel can improve [38,73,98,106]. This phenomenon exhibited that the MVF has considerable effect on the strengthening of DP steel. Concerning Equation (17), MVF strengthening is usually directly proportional to the MVF [38,42,53]:

$$\Delta\sigma_{\text{MVF}} \propto \text{MVF} \tag{17}$$

As a result of Equations (18) [107] and (19) [108], the hardness and strength of DP steels are the functions of MVF. Based on these equations, the hardness and strength are directly proportional to MVF, as follow [107,108]:

$$H_{F/M} = H_F V_F + H_M V_M = H_F + (H_M - H_F) V_M \quad (18)$$

$$\sigma_C = \sigma_\alpha V_\alpha + \sigma_M V_M = \sigma_\alpha + (\sigma_M - \sigma_\alpha) V_M \quad (19)$$

where $H_{F/M}$, H_F, H_M, σ_C, σ_α, σ_M, V_F, and V_M are the hardness of DP steel, ferrite hardness, martensite hardness, the strength of DP steel, ferrite strength, martensite strength, the volume fraction of ferrite, and MVF, respectively. It is worthy to note that typically an increase in strength causes a decrease in ductility. However, in some cases, increasing the MVF from an optimal value results in increasing strength and ductility, simultaneously. The increased ductility can be attributed to martensite softening [38,73]. By the increase in the MVF, the concentration of solute carbon in martensite decreases, leading to a decrease in its hardness and strength. In this way, martensite softening reduces the strength of DP steel [38,73]. It is worthy to note that there are various techniques for governing MVF and promoting MVF strengthening, which are presented in the following sections.

(1) The intercritical annealing temperature: a greater volume fraction of austenite is formed in the $\alpha + \gamma$ region by increasing the intercritical annealing temperature, resulting in an increasing MVF [44,47,73,109,110].

(2) The intercritical annealing time: The effect of intercritical annealing time in the $\alpha + \gamma$ zone is similar to that of intercritical annealing temperature. So, increasing the intercritical annealing time commonly increases the MVF [89,111].

(3) Chemical composition: The most momentous effectiveness of alloying elements on DP steels is changing the temperature range of the $\alpha + \gamma$ zone (i.e., the critical temperatures of A_1 and A_3) and governing the sensitivity level of the volume fraction of phases to the intercritical annealing temperature [1,2,50,112–114]. The carbon content of eutectoid point in the Fe–C phase diagram plays an important role in the volume fraction of phases [13]. During cooling from the dual-phase zone of $\alpha + \gamma$, the austenite hardenability, fraction of newly formed ferrite, and start temperature of martensitic transformation (M_s) are also the basic factors that are affected by chemical composition [1,2]. The carbon concentration of austenite is the main factor controlling the phase stability during cooling from the intercritical zone, which is noteworthy in two aspects [2]: (a) the carbon concentration of the primary austenite that is specified by the heating variables and the existence of carbide-creating elements and (b) the carbon concentration of the final austenite before transforming into martensite that depends on the fraction of newly transformed ferrite. Alloying elements that promote austenite hardenability and prohibit new ferrite creation could elevate M_s. This is on account of the depleting carbon concentration of the retained austenite [2].

The carbon element considerably affects the critical temperatures of A_1 and A_3 [1,2,114]. It is said that decreasing the carbon content can result in a decrease in the variation rate of the austenite/martensite fraction [2]. On the other hand, increasing the carbon content of steel also causes an increase in the MVF due to the decreasing temperature of A_3 [2,114]. The intercritical temperature range (i.e., the $\alpha + \gamma$ zone) can tremendously increase via silicon and aluminum compared to other alloying elements [2,12,13]. Thus, the variation rate of the austenite fraction/MVF is reduced with the intercritical annealing temperature [2]. The austenite hardenability increases via the increasing silicon content that results from the substantial increment of manganese partitioning between phases of ferrite and austenite/martensite [109]. A_1 temperature is increased via increasing the silicon content, and the slope of the solubility line of $\gamma/\alpha + \gamma$, i.e., A_3 temperature, increases with silicon as well. Thus, the $\alpha + \gamma$ zone becomes more widespread [13]. Increasing the silicon content decreases the carbon content of the eutectoid point [13]. Consequently, in a constant intercritical annealing temperature and time, the formed volume fraction of austenite, i.e., MVF, is reduced by increasing the silicon content [13,49,50]. M_S is enhanced

by an aluminum addition. This is valid, as quenching is carried out from the upper critical zone [2]. Meanwhile, at lower cooling rates, the creation of new ferrite can be facilitated via increasing the aluminum content. In this way, the carbon concentration of retained austenite will increase, leading to a reduction in M_s [2]. Aluminum will meaningfully increase the temperature of A_3. Hence, an increase in aluminum content at a constant intercritical annealing temperature could accelerate new ferrite creation and cause a decrease in the austenite fraction (i.e., MVF) [2]. It was also said that increasing the aluminum content could decrease the size of the martensite islands caused by more fractions of the newly created ferrite and decrease M_S for the retained austenite, in addition to the ferrite grain refinement [2]. The new ferrite will be formed via increasing the manganese content at lower temperatures and cooling rates [2]. On the other hand, increasing the manganese content increases the MVF. The reason for this can likely be attributed to the decreasing the temperature of A_1 and the carbon content of the eutectoid point [2]. The transformation of austenite to martensite is facilitated by a molybdenum addition at lower cooling rates. Accordingly, ferritic transformation is initiated at lower cooling rates via molybdenum addition, and bainitic transformation is also postponed. As a consequence, molybdenum increases the austenite hardenability, leading to an increase in the MVF [2]. The impact of chromium is similar to that of molybdenum; chromium addition results in the enhancement of austenite hardenability and the delay of ferrite transformation kinetics [2]. It was understood that the boron element could increase the austenite hardenability and increase the MVF, owing to the reduced fraction of the newly formed ferrite [2,9]. Boron can exist in terms of a solid solution and as boron carbide at the grain boundaries, causing retardation in the formation of the ferrite, pearlite, and bainite [9]. It is noteworthy that boron segregation or boron carbide precipitating at the grain boundaries decreases the energy of the grain boundaries, preventing the ferrite nucleation at these places. So, the hardenability is enhanced [9]. In this way, it can be concluded that the MVF could increase via boron addition [9]. Microalloying elements in DP steels can cause precipitation strengthening in addition to grain refinement [2,95]. An increase in the MVF via increased niobium content has also been reported [2,4]. In general, ferrite and austenite stabilizer elements can control the MVF.

(4) The density of nucleation sites for austenite in the $\alpha + \gamma$ zone: The density of suitable sites for austenite nucleation plays an effective role in MVF. A greater volume fraction of austenite is created in the $\alpha + \gamma$ region via increasing the density of these sites. Accordingly, the MVF will be increased [53,93]. The following processing routes can increase the density of these sites: (I) Cold rolling of a ferritic–pearlitic steel, followed by intercritical annealing treatment: With this processing route, similar to processing route 9 and 10 in FGS reduction, an increase in the density of the nucleation sites for austenite is associated with increasing the density of the ferrite/pearlite interface [53]. A fraction of nano-sized carbides located in the recrystallized ferrite grain boundaries are created if subcritical annealing below A_1 temperature is carried out [38,53]. These are the most potent nucleation sites for austenite during intercritical annealing [53]. In this way, a high MVF is obtained. Increasing the rolling reduction also increases the nucleation sites of austenite, resulting in an increasing MVF [53]. (II) Hot rolling of a ferritic–pearlitic steel below A_1 temperature, followed by intercritical annealing treatment: Hot rolling causes the formation of laminate ferrite and pearlite, as well as the spheroidized carbides located at the ferrite grain boundaries [93]. These carbides are the most potent nucleation sites for austenite. Via intercritical annealing, austenite is created through the dissolution of carbides, and a high MVF is obtained [93]. Increasing the rolling reduction will increase the carbides fraction with a higher degree of spheroidization, number of interface triple junctions, and fast diffusion routes (i.e., grain boundaries). As a consequence, the MVF is enhanced by increasing the rolling reduction [93]. (III) The heating rate during intercritical annealing treatment: It has been revealed that high heating rates during intercritical annealing could increase the MVF [115]. Its cause can be attributed to the prevalence of the austenite growth process over its nucleation process [115].

4.3. MM Contribution on the Strengthening

MM is another momentous factor that affects the strength of the matrix phase and DP steel [42,52,70]. The morphological effects of martensite are intricate, and unlike FGS and MVF, the same trend for them cannot be considered. There are three morphologies for the martensite phase in DP steels, consisting of (I) globular, (II) fine and fibrous, and (III) coarse islands (blocky and banded-shaped) [42,52,70]. These are produced by three different heat treatment cycles that are presented in the following sections.

(1) Intercritical annealing (IA): As can be seen in Figure 7a, in this cycle, the initial microstructure of steel consists of ferrite and pearlite (as normalized). By annealing in the $\alpha + \gamma$ zone, austenite is formed in the ferrite/carbide interface into the pearlite colonies. By dissolution of the carbides, austenite nucleases grow into the carbides. Then, austenite is transformed into the martensite phase via quenching. As a result, the resulting microstructure has the ferrite phase and the martensite phase with the globular and equiaxed morphology [52,70]. This martensite morphology is shown in Figure 7b [38].

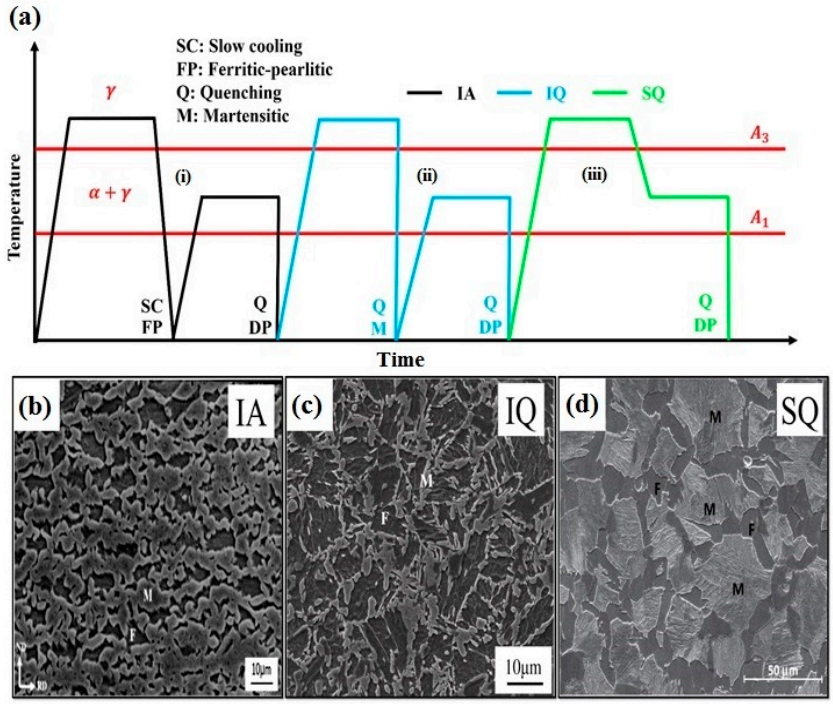

Figure 7. (**a**) Various heat treatment regimes for generation of different MMs in DP steels: (i) IA, (ii) IQ, and (iii) SQ. Various MMs in DP steels: (**b**) globular [38], (**c**) fibrous [66], and (**d**) coarse islands [116]. F = ferrite and M = martensite. Reprinted with permission from refs. [38,66,116]. Copyright 2021 Elsevier.

(2) Intermediate quenching (IQ): According to Figure 7a, in this cycle, at first, steel is fully austenitized and undergoes quenching. Therefore, the initial microstructure is fully martensitic. Then, steel is intercritically annealed in the $\alpha + \gamma$ zone and both ferrite and austenite phases are created and grow into a needle shape along the lath boundaries of the martensite and PAGBs. Finally, austenite is transformed into martensite by quenching. The ultimate microstructure is also composed of the ferrite phase and martensite phase with the morphology of fine and fibrous [52,70]. This martensite morphology can be seen in Figure 7c [66].

(3) Step quenching (SQ): Based on Figure 7a, in this cycle, firstly, steel is fully austenitized. Then, the annealing temperature is reduced to the $\alpha + \gamma$ region. Thus, ferrite is formed in the PAGBs and grows into them. Finally, steel is subjected to quenching and austenite is transformed into martensite. The final microstructure consists of the

ferrite phase and martensite phase with the characteristic of coarse islands (blocky and banded) [3,52,70]. This martensite morphology is shown in Figure 7d [116].

These MMs have different special areas [42,52]. For this reason, there will be various areas of the ferrite/martensite interface, causing different volumetric expansion amounts and strains generated by martensitic transformation [42,52]. Hence, the ferrite phase will experience different plastic strains, and various densities of dislocations will be made inside ferrite [42,52]. Moreover, this can likely be effective in reducing the mean free path and the pinning effect of the grain boundaries of ferrite [42,52]. This expresses the substantial role of MM (size, shape, distribution) on the mechanical behavior of DP steel. It has been concluded that the promotion of MM strengthening is in the order of globular, fibrous, and coarse islands [52]. However, it was reported in another work that the globular morphology causes higher strengthening as compared to the fibrous morphology [116,117]. On the other hand, a completely different conclusion from the aforementioned results was described in another research, so that an increase in MM strengthening was in the order of coarse islands, globular, and fibrous [42,117]. The reason for this trend is related to the microstructure refinement, i.e., the reduction of martensite size, FGS, and the mean free path of ferrite [42]. Accordingly, it cannot be argued with certainty that MM has a great contribution to the strengthening and strengthening corresponding to each of the MM alters, depending on the conditions. Equation (20) indicates that MM strengthening is a function of the martensite shape [42,52]:

$$\Delta\sigma_{\mathrm{MM}} \propto \beta_M. \tag{20}$$

where β_M is the martensite shape. This contains the geometry and dimensions of martensite.

5. Mechanical Properties of the DP Steels Affected by Strengthening Factors

Microstructural characteristics of the DP steels control the mechanical properties via interference in the strengthening mechanisms [13,52,76,89]. Therefore, it is required to study their effects on mechanical behavior. In this section, some important case studies will be described. Calcagnotto et al. [48] investigated the effect of ferrite refinement on the behavior of DP steels. They created DP steels with CG ferrite (12.4 μm), FG ferrite (2.4 μm), and UFG ferrite (1.2 μm). The tensile properties were reported in Table 1 [48]. It can be said that both yield and ultimate tensile strength are increased by a decrease in FGS. The reason for it corresponds to FGS strengthening. According to Equation (8), two terms of $\Delta\sigma_{MVF}$ and $\Delta\sigma_{MM}$ can be ignored and only the term of $\Delta\sigma_{FGS}$ has a significant role in the strengthening. However, ductility (uniform and total elongation) does not tolerate noticeable changes via the reduction of FGS. This can be attributed to an increase in the primary work hardening rate [48]. The work hardening exponent obtained by the Hollomon relation is presented in Table 1 [48]. The work hardening exponent for CG ferrite is 0.21. However, this is slightly lower for FG and UFG ferrite (i.e., 0.18). The reason for this can be due to slight and inappreciable changes in uniform elongation via ferrite grain refinement [48]. Figure 8a–c demonstrate the fracture surfaces after the tensile test [48]. It can be seen that the fracture surface related to CG ferrite is mainly composed of cleavage characteristics. This is referred to by the martensite cracking caused by its lower toughness, further tolerance of the applied stresses via this phase, and existence of former austenite/austenite grain boundaries. In the fracture surface corresponding to FG ferrite, the dimples fraction is greater than that of cleavage. Moreover, the fracture surface of UFG ferrite mostly includes dimples. The fracture behavior that improved with ferrite grain refinement can be a result of the promotion of martensite plasticity, less possibility of martensite cracking, less endurance of stresses by it due to more ferrite grains, and smaller, more spherical, and more uniform martensite islands. It should be noted that the high density of ferrite grain boundaries via grain refinement is also a very operative barrier to prevent crack propagation. Consequently, a more ductile fracture will be obtained [48].

Table 1. Tensile properties of DP steels with different FGSs [48]. Reprinted with permission from ref. [48]. Copyright 2021 Elsevier.

Steel	MVF (%)	FGS (μm)	YS (MPa)	UTS (MPa)	UE (%)	TE (%)	*n*-Value
CG	31.3	12.4	445 ± 17	870 ± 25	7.2 ± 0.7	7.7 ± 1.0	0.21 ± 0.01
FG	30.1	2.4	483 ± 7	964 ± 4	7.4 ± 0.4	8.9 ± 0.8	0.18 ± 0.01
UFG	29.8	1.2	525 ± 8	1037 ± 15	7.1 ± 0.5	7.3 ± 0.4	0.18 ± 0.01

CG = coarse-grained, FG = fine-grained, UFG = ultrafine-grained, YS = yield strength, UTS = ultimate tensile strength, UE = uniform elongation, TE = total elongation, and *n* = work hardening exponent according to the Hollomon relation.

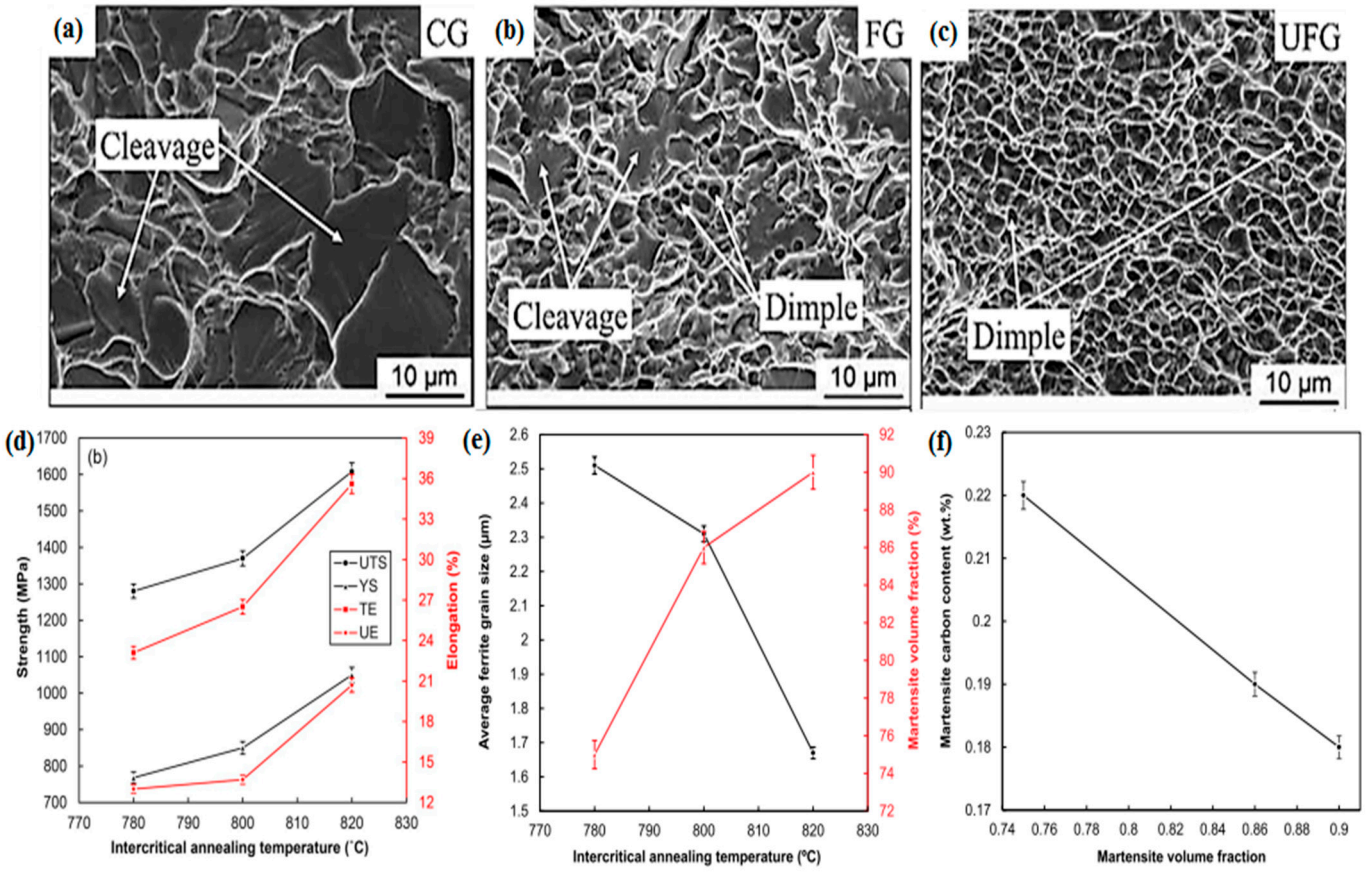

Figure 8. (**a**–**c**) Fractography via SEM after tensile test for DP steels with different FGSs [48], (**d**) tensile properties, (**e**) average FGS and MVF as a function of intercritical annealing temperature, and (**f**) relationship between martensite carbon content and MVF [73]. WQ = water quenching and WR = warm rolling. Reprinted with permission from refs. [48,73]. Copyright 2021 Elsevier.

Gao et al. [93] evaluated the effect of warm rolling and intercritical annealing temperature on the mechanical properties of DP steels (such as processing route seven in Figure 5h). Their results revealed that the MVF increases and FGS decreases with increasing intercritical annealing temperatures from 780–840 °C at a constant rolling reduction. On the other hand, at a constant intercritical annealing temperature, an increment in the rolling reduction from 40% to 60% also leads to an increase in the MVF and a decrease in FGS. Their result also showed that at an identical rolling reduction and increasing intercritical annealing temperature from 780 to 840 °C caused an increase in both yield and ultimate tensile strength and a decrease in ductility as a result of the effective role of MVF and FGS in mechanical performance. It should be said that at an identical intercritical annealing temperature, an increment in the rolling reduction from 40 to 60%, led to a promotion in strength and a decrement in ductility as well. This is attributed to the MVF and FGS

contribution to the strengthening again. In this study, according to Equation (8), the term of $\Delta\sigma_{MM}$ can be disregarded, and the two terms of $\Delta\sigma_{FGS}$ and $\Delta\sigma_{MVF}$ simultaneously result in strengthening [93].

Das et al. [52] produced three DP steels with different MMs via IA (hardness: 253 ± 6 HV; UTS: 843 MPa), IQ (hardness: 266 ± 3 HV; UTS: 892 MPa), and SQ (hardness: 281 ± 4 HV; UTS: 931 MPa) cycles. It can be said that increasing the hardness and strength for various MMs is in the order of globular, fibrous, and coarse islands. In this case, it was concerning Equation (8), in which only the term of $\Delta\sigma_{MM}$ plays a dominant role in strengthening. Meanwhile, the promotion of ductility for different MMs is in the order of coarse islands, globular, and fibrous. Superior ductility of the fibrous morphology compared to other morphologies is probably due to less distance between regions of the martensite phase and its fine and random morphology, which delay microvoid growth and coalescence [52].

Wang et al. [55] developed DP steels with different intercritical annealing temperatures. Table 2 summarizes the tensile properties [55]. It is found that an increment of intercritical annealing temperature from 740 up to 780 °C causes an increase in strength and a decrease in ductility. This can be recognized via the changes in MVF caused by increasing the intercritical annealing temperature. So, the MVF is enhanced with an increase in the intercritical annealing temperature, resulting in an improvement in mechanical characteristics [55]. Regarding Equation (8), only the term of $\Delta\sigma_{MVF}$ plays an effective role in strengthening.

Table 2. Tensile properties of DP steels with different intercritical annealing temperatures [55]. Reprinted with permission from ref. [55]. Copyright 2021 Elsevier.

Steel	YS (MPa)	UTS (Mpa)	TE (%)
HA74 (740 °C)	574	851	15.98
HA76 (760 °C)	602	885	13.01
HA78 (780 °C)	621	914	11.03

YS = yield strength, UTS = ultimate tensile strength, TE = total elongation.

Dai et al. [21] evaluated the process of fast-heating annealing on cold-rolled DP980 steel, and their finding exhibited that fast-heating annealing could be a possible path to develop high-performance DP steels by using the benefit of austenite decomposition [21]. In addition, the discontinuous and ultrafine martensite phase encircled by the interconnected network ferrite phase was formed at a temperature of 1073 K for 100 s. In this respect, the cold-rolled DP980 steel is quickly austenitized above the temperature of full austenitization at a heating rate of 300 K/s with a high ultimate tensile strength (1204 MPa) and a fracture elongation (16.7%) [21]. Besides, the study of the fatigue behavior of DP steels is significant [118–122]. It has been revealed that the behavior of cyclic hardening and softening depends on the MVF. So, the cyclic hardening and cyclic softening take place in DP steels with low and high MVF, respectively [118]. The cyclic hardening and softening behavior can result from a complicated interaction between ferrite hardening and martensite softening [118]. It was reported that increasing the MVF causes an increase and a decrease in low cycle fatigue life at low total strain amplitude and high total strain amplitude, respectively [118]. On the other hand, it was shown that a high MVF leads to the creation of secondary cracks during fatigue crack propagation, decelerating crack advancement [40]. Martensite can also make a closing crack over the crack head, causing difficult propagation resulting from irregularities in connection with the crack advancement on the martensite phase [40]. Lian et al. [123] studied the damage behavior of DP steels under different stress states. Their finding exhibited that the damage initiation preferably takes place at the ferrite/martensite interface under conditions of equibiaxial tension, plane strain tension, and uniaxial tension either in the martensite phase with a sharp edge or in the center of two martensite islands close together [123].

Rudnizki et al. [124] demonstrated that the microstructural evolutions during the full processing route should be precisely governed to achieve the ideal mechanical properties for DP steel. Hence, they concluded that two and three-dimensional simulations of mi-

crostructural evolutions during the processing of DP steels could be recognized via the phase-field modeling method [124]. This provides a description of all metallurgical changes occurring on a microstructural scale during the intercritical annealing treatment, i.e., the austenite and the ferrite formation, and the recrystallization as a function of the process variables, initial microstructure, as well as the chemical composition could be considered. Bleck et al. [125] depicted that an optimized cooling strategy is required to form the desired microstructure of DP steel in the hot rolling process. Moreover, selecting an appropriate cooling procedure results in the fabrication of a DP steel with the desired distribution of the ferrite phase [125].

After a while, it is substantial to discuss the ductility of DP steels. An increment of MVF does not essentially decrease ductility. Mazaheri et al. [38] revealed that, in addition to strength, ductility also increases via an increase in the MVF from a certain value. They attributed the reason to a greater decrease in the concentration of the solute carbon in martensite by increasing the MVF [38]. Equation (21) also confirms that by increasing the MVF, the concentration of the dissolved carbon in martensite decreases [38]. Thus, the martensite is softened and becomes more deformable, causing an increase in ductility [38]:

$$C_m = \left[C - C_f(1 - V_m)\right] / V_m \tag{21}$$

where C, C_f, C_m, and V_m belong to the mean carbon content of DP steel, carbon content of ferrite, carbon content of martensite, and MVF, respectively. Jahanara et al. [73] exhibited that via increasing the intercritical annealing temperature from 780 to 820 °C, strength and ductility are simultaneously enhanced, as observed in Figure 8d [73]. It is noted that an increment of intercritical annealing temperature from 780 to 820 °C increases the MVF and decreases FGS, based on Figure 8e [73]. The reason for the increased strength can be described as a result of increasing FGS and MVF strengthening with an increasing intercritical annealing temperature. Meanwhile, the reason for increased ductility can result from [73]: (a) martensite softening caused by decreasing the solute carbon in it via increasing MVF, as seen in Figure 8f [73]; (b) an increase in the mean free path of martensite with an increasing MVF; (c) avoidance of spreading the strain localized in the ferrite grains to the adjacent ferrite grains via increased MVF with a chain-networked MM, and (d) a decrease in the difference between mechanical properties of ferrite and martensite through the reduction of FGS and an increment of MVF, causing an improvement in the cohesion of the ferrite/martensite interface and a postponement in the plastic instability, i.e., necking.

The hole expansion test (HET) assesses the stretch-flangeability property, in other words, the formability of a material that possesses a primary defect (i.e., the preliminary central hole) [18,44]. Hole expansion ratio (HER) can be calculated using Equation (22) [44]:

$$\text{HER } (\%) = \left(d_f - d_0/d_0\right) \times 100 \tag{22}$$

where d_0 and d_f are the initial and final hole diameter, respectively. It can be said that an increasing HER indicates an increase in the formability [44]. Yoon et al. [44] concluded that increasing the MVF leads to the escalation of HER. This could be related to the decreasing martensite carbon content and the improving martensite plasticity, as well as the reduction of the hardness difference between ferrite and martensite with increasing MVF [44]. On the other hand, their result also illustrated through the single-edge notched tensile (SENT) test that the fracture energy/resistance is enhanced with an increase in the MVF [44]. Therefore, their result reveals that the formability and fracture energy/resistance are simultaneously promoted by an increasing MVF [44].

It is worth noting that great ductility at a certain strength is one of the best properties of DP steels among AHSSs [1,2,105]. Based on the literature [2,105,111], the work hardening rate could control uniform elongation. It is said that improved uniform elongation is obtained by an increase in the work hardening exponent (n) or $d\sigma/d\varepsilon$ and/or the difference UTS-YS [1,2,111]. Ductility is extremely dependent on the MVF and carbon concentration

in martensite [38]. There is an experimental relation based on Equation (23) that links the true uniform strain of DP steel (ε_u^{DP}) and true uniform strain of the ferrite phase (ε_u^F) with the MVF (V_M) and carbon concentration in martensite (C_M) [2]:

$$\varepsilon_u^{DP}/\varepsilon_u^F = 1 - 2.2C_M(V_M)^{1/2} \quad (23)$$

It is clear that the effectiveness of C_M is more than that of V_M. Regarding Equation (23), uniform elongation can increase via decreasing C_M and V_M. In contrast, increasing C_M and V_M can decrease uniform elongation. In this respect, it was reported [38,73] that the carbon content of martensite is inversely changed by the MVF. Equation (23) describes how uniform elongation in DP steel is enhanced by decreasing C_M without an increment of V_M [2]. It was exhibited [38,73] that the ductility of DP steel is possibly improved by increasing the MVF in some cases. This was caused by reducing the carbon content of martensite (i.e., decreasing martensite hardness) and increasing martensite plasticity [38,73]. In this respect, Equation (23) further confirms the significant effect of carbon content on uniform elongation, where ferrite grain refinement can also boost martensite plasticity [48]. However, it has been stated that the ductility is lessened by an increase in the MVF at higher hardness of the martensite phase [2]. This is resulting from the rapid formation of voids as a result of the plastic deformation incompatibility between ferrite and martensite [2]. According to Equation (23), one of the most effective approaches for improving uniform elongation in DP steels is to enhance ε_u^F. On the other hand, at a constant MVF, the ductility of DP steel is also determined by the ferrite ductility [1,2]. An increase in MVF also causes a reduction in total elongation, such as uniform elongation. This could be attributed to the reduction in uniform elongation and lower post-necking strain (i.e., the difference TE-UE) [2]. Similarly, it was revealed that an increase in C_M (and the martensite hardness) leads to a decrease in the difference TE-UE, i.e., the step length of localized plastic deformation. This is referred to more often as facilitated decohesion/martensite failure [2]. There are differences in the total elongation related to DP steels at constant tensile strength and MVF that imply the importance of the size, continuity, distribution, and geometry of the martensite phase in the preliminary size of microvoids and the step length of localized plastic deformation (post-necking) before microvoid coalescence [1,2]. It was also demonstrated that the refined martensite phase caused the highest total elongation. This is a result of more uniform elongation and lesser size of voids, hindering their coalescence [2]. Overall, all factors such as FGS, MVF, and MM should be appropriately determined since the ferrite ductility, martensite plasticity, and work hardening exponent, which importantly control the ductility of DP steels, are impressed by these factors.

Strength–ductility balance (SDB) is a crucial feature that is strongly affected by grain size, phase volume fraction, and phase morphology [126–152]. This is estimated by Equation (24) [12,38]:

$$\text{SDB}\left(\text{J/cm}^3\right) = \text{UTS} \times \text{UE} \quad (24)$$

where UTS and UE are the ultimate tensile strength and uniform elongation, respectively. Regarding Equation (24), SDB is as a function of UTS and UE. Accordingly, the improvement of UTS and UE leads to the escalation of SDB [12]. All researchers and automobile engineers are attempting to promote SDB, since higher SDB represents the excellent mechanical performance of DP steel. Moreover, SDB also represents deformation energy, where the higher the SDB, the more energy absorption (deformation energy) [12]. It is so crucial to clarify that SDB contributes to the selection of optimum FGS, MVF, and MM. Thus, it has been confirmed that the highest SDB and the ideal mechanical performance can be acquired using a concurrent blend of optimized FGS and MVF, as well as favorable MM, as shown in Figure 9.

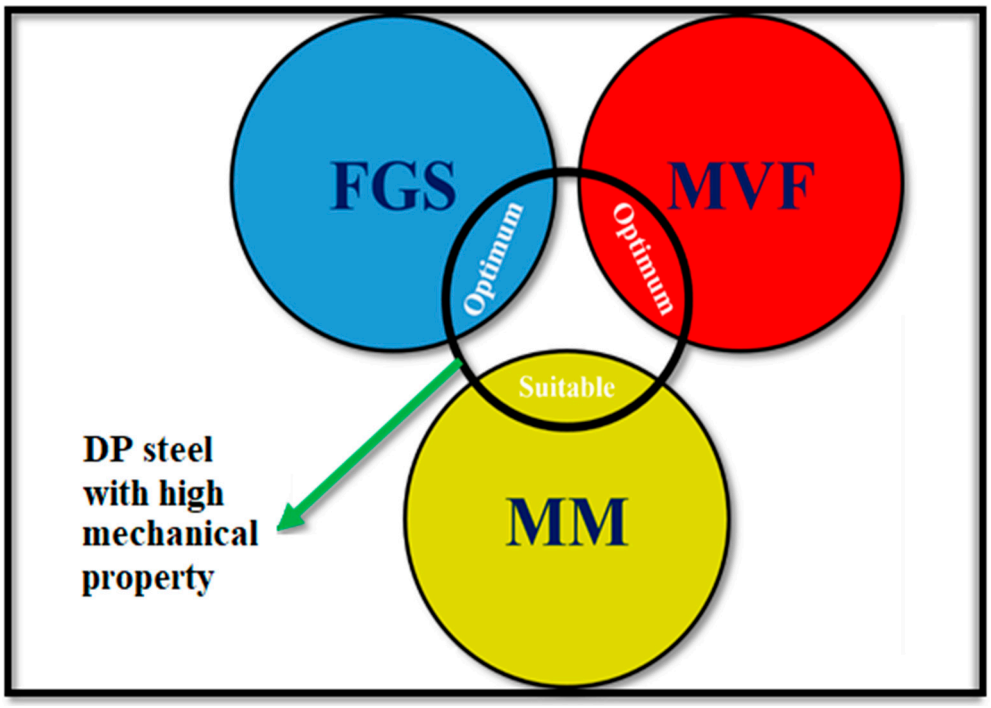

Figure 9. The role of FGS, MVF, and MM for achieving a DP steel with highest strength–ductility balance along with high mechanical properties.

6. Conclusions and the Future Outlook

This review paper aimed to introduce strengthening mechanisms and their processing routes in dual-phase (DP) steels. It was found that ferrite grain size (FGS), martensite volume fraction (MVF), and martensite morphology (MM) are the main microstructural characteristics in DP steels that strongly affect the mechanical properties. The cause is that each of these characteristics can solely result in a substantial strengthening. It has been confirmed that FGS, MVF, and MM are three primary factors that contribute to the strengthening of DP steels. Ultrahigh-strength DP steels can be developed with the help of these strengthening factors, which are very suitable for the automotive industry. There are many processing routes for altering the microstructural characteristics and further strengthening DP steels, which were mostly noted in this review article. Via focusing on these processing routes, it is possible to produce DP steels with a vast range of strength–ductility balance. The current review could present fundamental information to researchers and automotive engineers to create more novel techniques for the promotion of strengthening factors in DP steels with the aim of upgraded safety and mechanical response of automobiles against accidents. It has been confirmed that a banded microstructure can be created in DP steels, which weakens mechanical properties such as failure behavior. Thus, prevention of the banded microstructure formation could significantly promote DP steel performance. Friction stir processing may be desirable to modify the banded microstructure owing to the fragmentation of phases, homogenizing their distribution and grain refinement. Moreover, researchers should focus more attention on the effects of other alloying elements such as tungsten, tantalum, cobalt, etc., on the microstructures and mechanical properties of DP steels. Severe plastic deformation approaches, e.g., friction stir processing, accumulative roll bonding, equal channel angular pressing, etc., are also employed to refine these microstructures. It is proposed that the grain refinement approach be merged with severe plastic deformation to attain a nanograin structure. Martensite plasticity is very substantial for the ductility and failure behavior of DP steels. Thus, the formation of martensite with a higher plasticity can be an effective approach to escalate the functions of DP steels. Eventually, it is worth noting that achieving the strength–ductility balance of DP steels by

tailoring the microstructure is still controversial; hence, more studies should be conducted regarding this issue.

Author Contributions: Conceptualization, visualization, investigation, writing—original draft preparation, F.B. (Farzad Badkoobeh); Conceptualization, supervision, writing—review and editing, H.M., M.R. and H.R.B.-R.; supervision, writing—review and editing, funding acquisition, F.B. (Filippo Berto). All authors have read and agreed to the published version of the manuscript.

Funding: This research received no external funding.

Conflicts of Interest: The authors declare that they have no competing/financial conflicts of interest.

References

1. Tasan, C.C.; Diehl, M.; Yan, D.; Bechtold, M.; Roters, F.; Schemmann, L.; Zheng, C.; Peranio, N.; Ponge, D.; Koyama, M.; et al. An overview of dual-phase steels: Advances in microstructure-oriented processing and micromechanically guided design. *Annu. Rev. Mater. Res.* **2015**, *45*, 391–431. [CrossRef]
2. Fonstein, N. Dual-phase steels. In *Automotive Steels*; Woodhead Publishing: Cambridge, UK, 2017; pp. 169–216. [CrossRef]
3. Guo, C.; Hao, L.; Li, S.; Kang, Y.; An, Y. Effect of microstructure quenched around Ac3 point on the damage behavior in 0.087C–1.35Mn steel. *J. Mater. Res. Technol.* **2019**, *8*, 5103–5113. [CrossRef]
4. Kalashami, A.G.; Kermanpur, A.; Ghassemali, E.; Najafizadeh, A.; Mazaheri, Y. The effect of Nb on texture evolutions of the ultrafine-grained dual-phase steels fabricated by cold rolling and intercritical annealing. *J. Alloys Compd.* **2017**, *694*, 1026–1035. [CrossRef]
5. Yuan, Q.; Wang, Z.; Zhang, Y.; Ye, J.; Huang, Y.; Huang, A. Effect of Warm Rolling Temperature on the Microstructure and Texture of Microcarbon Dual-Phase (DP) Steel. *Metals* **2020**, *10*, 566. [CrossRef]
6. Mihaliková, M.; Zgodavová, K.; Bober, P.; Sütőová, A. Prediction of Bake Hardening Behavior of Selected Advanced High Strength Automotive Steels and Hailstone Failure Discussion. *Metals* **2019**, *9*, 1016. [CrossRef]
7. Kim, M.T.; Park, T.M.; Baik, K.-H.; Choi, W.S.; Han, J. Effects of cold rolling reduction ratio on microstructures and tensile properties of intercritically annealed medium-Mn steels. *Mater. Sci. Eng. A* **2019**, *752*, 43–54. [CrossRef]
8. Soleimani, M.; Kalhor, A.; Mirzadeh, H. Transformation-induced plasticity (TRIP) in advanced steels: A review. *Mater. Sci. Eng. A* **2020**, *795*, 140023. [CrossRef]
9. Kumar, S.; Desai, R. Effect of Boron Micro-alloying on Microstructure and Corrosion Behavior of Dual-Phase Steel. *J. Mater. Eng. Perform.* **2019**, *28*, 6228–6236. [CrossRef]
10. Zhou, Q.; Qian, L.; Meng, J.; Zhao, L. The fatigue properties, microstructural evolution and crack behaviors of low-carbon carbide-free bainitic steel during low-cycle fatigue. *Mater. Sci. Eng. A* **2021**, *820*, 141571. [CrossRef]
11. Liu, L.; Maresca, F.; Hoefnagels, J.; Vermeij, T.; Geers, M.; Kouznetsova, V. Revisiting the martensite/ferrite interface damage initiation mechanism: The key role of substructure boundary sliding. *Acta Mater.* **2020**, *205*, 116533. [CrossRef]
12. Badkoobeh, F.; Nouri, A.; Hassannejad, H. The bake hardening mechanism of dual-phase silicon steels under high pre-strain. *Mater. Sci. Eng. A* **2019**, *770*, 138544. [CrossRef]
13. Badkoobeh, F.; Nouri, A.; Hassannejad, H.; Mostaan, H. Microstructure and mechanical properties of resistance spot welded dual-phase steels with various silicon contents. *Mater. Sci. Eng. A* **2020**, *790*, 139703. [CrossRef]
14. Hou, Y.; Min, J.; Guo, N.; Lin, J.; Carsley, J.E.; Stoughton, T.B.; Traphöner, H.; Clausmeyer, T.; Tekkaya, A.E. Investigation of evolving yield surfaces of dual-phase steels. *J. Mater. Process. Technol.* **2021**, *287*, 116314. [CrossRef]
15. Wang, M.; Huang, M. Abnormal TRIP effect on the work hardening behavior of a quenching and partitioning steel at high strain rate. *Acta Mater.* **2020**, *188*, 551–559. [CrossRef]
16. Avishan, B.; Khoshkebari, S.M.; Yazdani, S. Effect of pre-existing martensite within the microstructure of nano bainitic steel on its mechanical properties. *Mater. Chem. Phys.* **2021**, *260*, 124160. [CrossRef]
17. Kumar, R.; Dwivedi, R.K.; Ahmed, S. Stability of Retained Austenite in Carbide Free Bainite during the Austempering Temperature and its Influence on Sliding Wear of High Silicon Steel. *Silicon* **2021**, *13*, 1249–1259. [CrossRef]
18. Thakur, A.K.; Kumar, R.R.; Bansal, G.K.; Verma, R.K.; Tarafder, S.; Sivaprasad, S.; Mandal, G.K. Processing-Microstructure-Property Correlation for Producing Stretch-Flangeable Grade Dual-Phase Steel. *J. Mater. Eng. Perform.* **2021**, *30*, 4300–4317. [CrossRef]
19. Li, S.; Guo, C.; Hao, L.; Kang, Y.; An, Y. Microstructure-Based Modeling of Mechanical Properties and Deformation Behavior of DP600 Dual Phase Steel. *Steel Res. Int.* **2019**, *90*, 1900311. [CrossRef]
20. Hu, X.; Ke, D.; Zhi, Y.; Liu, X. Effect of Two Steps Overaging on Mechanical Properties of Tailor Rolled Blank of Dual Phase Steel. *Metals* **2021**, *11*, 792. [CrossRef]
21. Dai, J.; Meng, Q.; Zheng, H. High-strength dual-phase steel produced through fast-heating annealing method. *Results Mater.* **2020**, *5*, 100069. [CrossRef]
22. Shan, Y.V.; Soliman, M.; Palkowski, H.; Kozeschnik, E. Modeling of Bake Hardening Kinetics and Carbon Redistribution in Dual-Phase Steels. *Steel Res. Int.* **2021**, *92*, 2000307. [CrossRef]

23. Çobanoğlu, M.; Ertan, R.K.; Şimşir, C.; Efe, M. Excessive damage increase in dual phase steels under high strain rates and temperatures. *Int. J. Damage Mech.* **2021**, *30*, 283–296. [CrossRef]
24. Davaze, V.; Vallino, N.; Feld-Payet, S.; Langrand, B.; Besson, J. Plastic and fracture behavior of a dual phase steel sheet under quasi-static and dynamic loadings. *Eng. Fract. Mech.* **2020**, *235*, 107165. [CrossRef]
25. Singh, M.; Das, A.; Venugopalan, T.; Mukherjee, K.; Walunj, M.; Nanda, T.; Kumar, B.R. Impact of Martensite Spatial Distribution on Quasi-Static and Dynamic Deformation Behavior of Dual-Phase Steel. *Met. Mater. Trans. A* **2018**, *49*, 463–475. [CrossRef]
26. An, D.; Baik, S.-I.; Ren, Q.; Jiang, M.; Zhu, M.; Isheim, D.; Krakauer, B.W.; Seidman, D.N. A transmission electron microscopy and atom-probe tomography study of martensite morphology and composition in a dual-phase steel. *Mater. Charact.* **2020**, *162*, 110207. [CrossRef]
27. Asadipoor, M.; Kadkhodapour, J.; Anaraki, A.P.; Sharifi, S.M.H.; Darabi, A.C.; Barnoush, A. Experimental and Numerical Investigation of Hydrogen Embrittlement Effect on Microdamage Evolution of Advanced High-Strength Dual-Phase Steel. *Met. Mater. Int.* **2021**, *27*, 2276–2291. [CrossRef]
28. Zhou, L.-Y.; Zhang, D.; Liu, Y.-Z. Influence of silicon on the microstructures, mechanical properties and stretch-flangeability of dual phase steels. *Int. J. Miner. Met. Mater.* **2014**, *21*, 755–765. [CrossRef]
29. Chen, C.-Y.; Li, C.-H.; Tsao, T.-C.; Chiu, P.-H.; Tsai, S.-P.; Yang, J.-R.; Chiang, L.-J.; Wang, S.-H. A novel technique for developing a dual-phase steel with a lower strength difference between ferrite and martensite. *Mater. Today Commun.* **2020**, *23*, 100895. [CrossRef]
30. Sun, J.; Jiang, T.; Wang, Y.; Guo, S.; Liu, Y. Ultrafine grained dual-phase martensite/ferrite steel strengthened and toughened by lamella structure. *Mater. Sci. Eng. A* **2018**, *734*, 311–317. [CrossRef]
31. Ramazani, A.; Ebrahimi, Z.; Prahl, U. Study the effect of martensite banding on the failure initiation in dual-phase steel. *Comput. Mater. Sci.* **2014**, *87*, 241–247. [CrossRef]
32. Lai, Q.; Bouaziz, O.; Gouné, M.; Perlade, A.; Bréchet, Y.; Pardoen, T. Microstructure refinement of dual-phase steels with 3.5 wt% Mn: Influence on plastic and fracture behavior. *Mater. Sci. Eng. A* **2015**, *638*, 78–89. [CrossRef]
33. Song, E.; Lee, G.-H.; Jeon, H.; Park, B.J.; Lee, J.-G.; Kim, J.-Y. Stretch-flangeability correlated with hardness distribution and strain-hardenability of constituent phases in dual- and complex-phase steels. *Mater. Sci. Eng. A* **2021**, *817*, 141353. [CrossRef]
34. Roodgari, M.R.; Jamaati, R.; Aval, H.J. A new method to produce dual-phase steel. *Mater. Sci. Eng. A* **2021**, *803*, 140695. [CrossRef]
35. Ramazani, A.; Mukherjee, K.; Prahl, U.; Bleck, W. Transformation-Induced, Geometrically Necessary, Dislocation-Based Flow Curve Modeling of Dual-Phase Steels: Effect of Grain Size. *Met. Mater. Trans. A* **2012**, *43*, 3850–3869. [CrossRef]
36. Ramazani, A.; Mukherjee, K.; Schwedt, A.; Goravanchi, P.; Prahl, U.; Bleck, W. Quantification of the effect of transformation-induced geometrically necessary dislocations on the flow-curve modelling of dual-phase steels. *Int. J. Plast.* **2013**, *43*, 128–152. [CrossRef]
37. Chen, Y.; Wu, Z.; Wu, G.; Wang, N.; Zhao, Q.; Luo, J. Investigation on micromechanism of ferrite hardening after pre-straining with different strain rates of dual-phase steel. *Mater. Sci. Eng. A* **2020**, *802*, 140657. [CrossRef]
38. Mazaheri, Y.; Jahanara, A.H.; Sheikhi, M.; Kalashami, A.G. High strength-elongation balance in ultrafine grained ferrite-martensite dual phase steels developed by thermomechanical processing. *Mater. Sci. Eng. A* **2019**, *761*, 138021. [CrossRef]
39. Frómeta, D.; Cuadrado, N.; Rehrl, J.; Suppan, C.; Dieudonné, T.; Dietsch, P.; Calvo, J.; Casellas, D. Microstructural effects on fracture toughness of ultra-high strength dual phase sheet steels. *Mater. Sci. Eng. A* **2021**, *802*, 140631. [CrossRef]
40. Velasquez, C.P.; Rodriguez, D.A.; Tovar, C.N.; Roncery, L.M.; Baracaldo, R.R. Fatigue Crack Growth and Fracture Toughness in a Dual Phase Steel: Effect of Increasing Martensite Volume Fraction. *Int. J. Automot. Mech. Eng.* **2020**, *17*, 8086–8095. [CrossRef]
41. Huan, P.-C.; Wang, X.-N.; Yang, L.; Zheng, Z.; Hu, Z.-R.; Zhang, M.; Chen, C.-J. Effect of Martensite Content on Failure Behavior of Laser Welded Dual-Phase Steel Joints During Deformation. *J. Mater. Eng. Perform.* **2019**, *28*, 1801–1809. [CrossRef]
42. Soliman, M.; Palkowski, H. Strain Hardening Dependence on the Structure in Dual-Phase Steels. *Steel Res. Int.* **2021**, *92*, 2000518. [CrossRef]
43. Calcagnotto, M.; Ponge, D.; Raabe, D. Effect of grain refinement to 1μm on strength and toughness of dual-phase steels. *Mater. Sci. Eng. A* **2010**, *527*, 7832–7840. [CrossRef]
44. Yoon, J.I.; Jung, J.; Lee, H.H.; Kim, J.Y.; Kim, H.S. Relationships Between Stretch-Flangeability and Microstructure-Mechanical Properties in Ultra-High-Strength Dual-Phase Steels. *Met. Mater. Int.* **2019**, *25*, 1161–1169. [CrossRef]
45. Das, H.; Mondal, M.; Hong, S.-T.; Lim, Y.; Lee, K.-J. Comparison of microstructural and mechanical properties of friction stir spot welded ultra-high strength dual phase and complex phase steels. *Mater. Charact.* **2018**, *139*, 428–436. [CrossRef]
46. Mostaan, H.; Saeedpour, P.; Ahmadi, H.; Nouri, A. Laser welding of dual-phase steels with different silicon contents: Phase evolutions, microstructural observations, mechanical properties, and fracture behavior. *Mater. Sci. Eng. A* **2021**, *811*, 140974. [CrossRef]
47. Nouri, A.; Saghafian, H.; Kheirandish, S. Influence of volume fraction of martensite on the work hardening behaviour of two dual-phase steels with high and low silicon contents. *Int. J. Mater. Res.* **2010**, *101*, 1286–1292. [CrossRef]
48. Calcagnotto, M.; Adachi, Y.; Ponge, D.; Raabe, D. Deformation and fracture mechanisms in fine- and ultrafine-grained ferrite/martensite dual-phase steels and the effect of aging. *Acta Mater.* **2011**, *59*, 658–670. [CrossRef]
49. Nouri, A.; Hassannejad, H.; Farrokhi-Rad, M. Relationship between Microstructure and Corrosion Behavior in Dual-Phase Steels with Various Si Content. *Steel Res. Int.* **2019**, *90*, 1900331. [CrossRef]

50. Nouri, A.; Hassannejad, H.; Farrokhi-Rad, M. Effect of Silicon Content on the Wear Behavior of Low-Carbon Dual-Phase Steels. *Tribol. Lett.* **2019**, *67*, 69. [CrossRef]
51. Khosravani, A.; Cecen, A.; Kalidindi, S.R. Development of high throughput assays for establishing process-structure-property linkages in multiphase polycrystalline metals: Application to dual-phase steels. *Acta Mater.* **2017**, *123*, 55–69. [CrossRef]
52. Das, D.; Chattopadhyay, P.P. Influence of martensite morphology on the work-hardening behavior of high strength ferrite–martensite dual-phase steel. *J. Mater. Sci.* **2009**, *44*, 2957–2965. [CrossRef]
53. Mazaheri, Y.; Jahanara, A.H.; Sheikhi, M.; Ghassemali, E. On the Simultaneous Improving of Strength and Elongation in Dual Phase Steels via Cold Rolling. *Metals* **2020**, *10*, 1676. [CrossRef]
54. Ebrahimi, F.; Saeidi, N.; Raeissi, M. Microstructural Modifications of Dual-Phase Steels: An Overview of Recent Progress and Challenges. *Steel Res. Int.* **2020**, *91*, 2000178. [CrossRef]
55. Wang, H.-S.; Yuan, G.; Kang, J.; Cao, G.; Li, C.-G.; Misra, R.; Wang, G. Microstructural evolution and mechanical properties of dual phase steel produced by strip casting. *Mater. Sci. Eng. A* **2017**, *703*, 486–495. [CrossRef]
56. Jung, J.; Yoon, J.I.; Park, H.K.; Kim, J.Y.; Kim, H.S. Bayesian approach in predicting mechanical properties of materials: Application to dual phase steels. *Mater. Sci. Eng. A* **2019**, *743*, 382–390. [CrossRef]
57. Ashrafi, H.; Shamanian, M.; Emadi, R.; Saeidi, N. Examination of phase transformation kinetics during step quenching of dual phase steels. *Mater. Chem. Phys.* **2017**, *187*, 203–217. [CrossRef]
58. Ji, D.; Zhang, M.; Zhu, D.; Luo, S.; Li, L. Influence of microstructure and pre-straining on the bake hardening response for ferrite-martensite dual-phase steels of different grades. *Mater. Sci. Eng. A* **2017**, *708*, 129–141. [CrossRef]
59. Calcagnotto, M.; Ponge, D.; Demir, E.; Raabe, D. Orientation gradients and geometrically necessary dislocations in ultrafine grained dual-phase steels studied by 2D and 3D EBSD. *Mater. Sci. Eng. A* **2010**, *527*, 2738–2746. [CrossRef]
60. Li, S.; Guo, C.; Hao, L.; Kang, Y.; An, Y. In-situ EBSD study of deformation behaviour of 600 MPa grade dual phase steel during uniaxial tensile tests. *Mater. Sci. Eng. A* **2019**, *759*, 624–632. [CrossRef]
61. Atreya, V.; Bos, C.; Santofimia, M.J. Understanding ferrite deformation caused by austenite to martensite transformation in dual phase steels. *Scr. Mater.* **2021**, *202*, 114032. [CrossRef]
62. Saha, D.; Biro, E.; Gerlich, A.; Zhou, Y. Influences of blocky retained austenite on the heat-affected zone softening of dual-phase steels. *Mater. Lett.* **2020**, *264*, 127368. [CrossRef]
63. Saleh, M.; Priestner, R. Retained austenite in dual-phase silicon steels and its effect on mechanical properties. *J. Mater. Process. Technol.* **2001**, *113*, 587–593. [CrossRef]
64. Dong, X.; Shen, Y.; Xue, W.; Jia, N. Improved work hardening of a medium carbon-TRIP steel by partial decomposition of retained austenite. *Mater. Sci. Eng. A* **2021**, *803*, 140504. [CrossRef]
65. Soliman, M.; Shan, Y.V.; Mendez-Martin, F.; Kozeschnik, E.; Palkowski, H. Strain aging characterization and physical modelling of over-aging in dual phase steel. *Mater. Sci. Eng. A* **2020**, *788*, 139595. [CrossRef]
66. Zhang, J.; Di, H.; Deng, Y.; Misra, R. Effect of martensite morphology and volume fraction on strain hardening and fracture behavior of martensite–ferrite dual phase steel. *Mater. Sci. Eng. A* **2015**, *627*, 230–240. [CrossRef]
67. Liu, J.; Jiang, Z.; Lian, J. Influence of predeformation on microstructure and mechanical properties of 1020 dual phase steel. *Mater. Sci. Technol.* **1991**, *7*, 527–532. [CrossRef]
68. Dieter, G.E. *Mechanical Metallurgy*, 3rd ed.; MCgraw-Hill Book Company: London, UK, 1988.
69. Hertzberg, R.W.; Vinci, R.P.; Hertzberg, J.L. *Deformation and Fracture Mechanics of Engineering Materials*, 5th ed.; John Wiley & Sons, Inc.: Hoboken, NJ, USA, 2013.
70. Trevisiol, C.; Jourani, A.; Bouvier, S. Effect of Martensite Morphology on Tribological Behaviour of a Low-Alloy Steel. *Met. Microstruct. Anal.* **2019**, *8*, 123–134. [CrossRef]
71. Singh, V.; Adhikary, M.; Venugopalan, T.; Chakraborty, A.; Nanda, T.; Kumar, B.R. Role of Recrystallization and Pearlite Dissolution in Industrial Processing of DP590 Steels. *Mater. Manuf. Process.* **2017**, *4*, 686–1816. [CrossRef]
72. Fan, S.; Hao, H.; Zhang, X.; Han, Q. Improvement in Mechanical Properties of a Surface-Carburized Ferrite–Martensite Dual-Phase Steel by Intercritical Annealing. *J. Mater. Eng. Perform.* **2020**, *29*, 7034–7044. [CrossRef]
73. Jahanara, A.H.; Mazaheri, Y.; Sheikhi, M. Correlation of ferrite and martensite micromechanical behavior with mechanical properties of ultrafine grained dual phase steels. *Mater. Sci. Eng. A* **2019**, *764*, 138206. [CrossRef]
74. Sun, J.; Jiang, T.; Sun, Y.; Wang, Y.; Liu, Y. A lamellar structured ultrafine grain ferrite-martensite dual-phase steel and its resistance to hydrogen embrittlement. *J. Alloys Compd.* **2017**, *698*, 390–399. [CrossRef]
75. Son, Y.I.; Lee, Y.K.; Park, K.-T.; Lee, C.S.; Shin, D.H. Ultrafine grained ferrite–martensite dual phase steels fabricated via equal channel angular pressing: Microstructure and tensile properties. *Acta Mater.* **2005**, *53*, 3125–3134. [CrossRef]
76. Mazaheri, Y.; Kermanpur, A.; Najafizadeh, A. Strengthening Mechanisms of Ultrafine Grained Dual Phase Steels Developed by New Thermomechanical Processing. *ISIJ Int.* **2015**, *55*, 218–226. [CrossRef]
77. Bag, A.; Ray, K.K.; Dwarakadasa, E.S. Influence of martensite content and morphology on tensile and impact properties of high-martensite dual-phase steels. *Met. Mater. Trans. A* **1999**, *30*, 1193–1202. [CrossRef]
78. Avendaño-Rodríguez, D.; Granados, J.D.; Espejo-Mora, E.; Mujica-Roncery, L.; Baracaldo, R.R. Fracture mechanisms in dual-phase steel: Influence of martensite volume fraction and ferrite grain size. *J. Eng. Sci. Technol. Rev.* **2018**, *11*, 174–181. [CrossRef]
79. Hai, C.; Cheng, X.; Du, C.; Li, X. Role of Martensite Structural Characteristics on Corrosion Features in Ni-Advanced Dual-Phase Low-Alloy Steels. *Acta Met. Sin. Engl. Lett.* **2021**, *34*, 802–812. [CrossRef]

80. Paul, S.K. Effect of martensite volume fraction on stress triaxiality and deformation behavior of dual phase steel. *Mater. Des.* **2013**, *50*, 782–789. [CrossRef]
81. Sarwar, M.; Priestner, R. Influence of ferrite-martensite microstructural morphology on tensile properties of dual-phase steel. *J. Mater. Sci.* **1996**, *31*, 2091–2095. [CrossRef]
82. Dutta, T.; Das, D.; Banerjee, S.; Saha, S.K.; Datta, S. An automated morphological classification of ferrite-martensite dual-phase microstructures. *Measurement* **2019**, *137*, 595–603. [CrossRef]
83. Ebrahimian, A.; Banadkouki, S.G. Mutual mechanical effects of ferrite and martensite in a low alloy ferrite-martensite dual phase steel. *J. Alloys Compd.* **2017**, *708*, 43–54. [CrossRef]
84. Rana, A.K.; Paul, S.K.; Dey, P.P. Effect of martensite volume fraction on cyclic plastic deformation behavior of dual phase steel: Micromechanics simulation study. *J. Mater. Res. Technol.* **2019**, *8*, 3705–3712. [CrossRef]
85. Jazaeri, H.; Humphreys, F.J. The transition from discontinuous to continuous recrystallization in some aluminium alloys. *Acta Mater.* **2004**, *52*, 3251–3262. [CrossRef]
86. Nasiri, Z.; Ghaemifar, S.; NaghiZadeh, M.; Mirzadeh, H. Thermal Mechanisms of Grain Refinement in Steels: A Review. *Met. Mater. Int.* **2021**, *27*, 2078–2094. [CrossRef]
87. Du, C.; Hoefnagels, J.; Kölling, S.; Geers, M.; Sietsma, J.; Petrov, R.; Bliznuk, V.; Koenraad, P.; Schryvers, D.; Amin-Ahmadi, B. Martensite crystallography and chemistry in dual phase and fully martensitic steels. *Mater. Charact.* **2018**, *139*, 411–420. [CrossRef]
88. Matsuyama, S.; Galindo-Nava, E.I. A Unified Model for Plasticity in Ferritic, Martensitic and Dual-Phase Steels. *Metals* **2020**, *10*, 764. [CrossRef]
89. Bakhtiari, M.; Kermanpur, A.; Han, J.; Najafizadeh, A. Effect of Intercritical Annealing on Microstructure and Tensile Properties of an Ultrafine-Grained Dual-Phase Low Alloy Steel Containing Titanium. *Steel Res. Int.* **2020**, *91*, 2000118. [CrossRef]
90. Pan, Z.; Gao, B.; Lai, Q.; Chen, X.; Cao, Y.; Liu, M.; Zhou, H. Microstructure and Mechanical Properties of a Cold-Rolled Ultrafine-Grained Dual-Phase Steel. *Materials* **2018**, *11*, 1399. [CrossRef]
91. Nikkhah, S.; Mirzadeh, H.; Zamani, M. Fine tuning the mechanical properties of dual phase steel via thermomechanical processing of cold rolling and intercritical annealing. *Mater. Chem. Phys.* **2019**, *230*, 1–8. [CrossRef]
92. Najafi, M.; Mirzadeh, H.; Alibeyki, M. Improved Mechanical Properties of Structural Steel via Developing Bimodal Grain Size Distribution and Intercritical Heat Treatment. *J. Mater. Eng. Perform.* **2019**, *28*, 5409–5414. [CrossRef]
93. Gao, B.; Hu, R.; Pan, Z.; Chen, X.; Liu, Y.; Xiao, L.; Cao, Y.; Li, Y.; Lai, Q.; Zhou, H. Strengthening and ductilization of laminate dual-phase steels with high martensite content. *J. Mater. Sci. Technol.* **2021**, *65*, 29–37. [CrossRef]
94. Ashrafi, H.; Shamanian, M.; Emadi, R.; Saeidi, N. A novel and simple technique for development of dual phase steels with excellent ductility. *Mater. Sci. Eng. A* **2017**, *680*, 197–202. [CrossRef]
95. Niakan, H.; Najafizadeh, A. Effect of niobium and rolling parameters on the mechanical properties and microstructure of dual phase steels. *Mater. Sci. Eng. A* **2010**, *527*, 5410–5414. [CrossRef]
96. Rajput, S.K.; Mehta, Y.; Chaudhari, G.P.; Nath, S.K. Optimized Thermomechanical Processing for Fine-Grained Dual-Phase Microstructure Using Deformation-Induced Ferrite Transformation. *J. Mater. Eng. Perform.* **2020**, *29*, 4260–4274. [CrossRef]
97. Aktarer, S.; Küçükömeroğlu, T.; Davut, K. Friction stir processing of dual phase steel: Microstructural evolution and mechanical properties. *Mater. Charact.* **2019**, *155*, 109787. [CrossRef]
98. Deng, Y.G.; Li, Y.; Di, H.; Misra, R.D.K. Effect of Heating Rate during Continuous Annealing on Microstructure and Mechanical Properties of High-Strength Dual-Phase Steel. *J. Mater. Eng. Perform.* **2019**, *28*, 4556–4564. [CrossRef]
99. Zhang, J.; Sun, Y.; Ji, Z.; Luo, H.; Liu, F. Improved mechanical properties of V-microalloyed dual phase steel by enhancing martensite deformability. *J. Mater. Sci. Technol.* **2021**, *75*, 139–153. [CrossRef]
100. Drumond, J.; Girina, O.; Filho, J.F.D.S.; Fonstein, N.; De Oliveira, C.A.S. Effect of Silicon Content on the Microstructure and Mechanical Properties of Dual-Phase Steels. *Met. Microstruct. Anal.* **2012**, *1*, 217–223. [CrossRef]
101. Mohrbacher, H.; Yang, J.-R.; Chen, Y.-W.; Rehrl, J.; Hebesberger, T. Metallurgical Effects of Niobium in Dual Phase Steel. *Metals* **2020**, *10*, 504. [CrossRef]
102. Calcagnotto, M.; Ponge, D.; Raabe, D. On the Effect of Manganese on Grain Size Stability and Hardenability in Ultrafine-Grained Ferrite/Martensite Dual-Phase Steels. *Met. Mater. Trans. A* **2012**, *43*, 37–46. [CrossRef]
103. Gotawala, N.; Wadighare, A.; Shrivastava, A. Phase transformation during friction stir processing of dual-phase 600 steel. *J. Mater. Sci.* **2020**, *55*, 4464–4477. [CrossRef]
104. Jiang, Z.; Guan, Z.; Lian, J. Effects of microstructural variables on the deformation behaviour of dual-phase steel. *Mater. Sci. Eng. A* **1995**, *190*, 55–64. [CrossRef]
105. Yaghoobi, F.; Jamaati, R.; Aval, H.J. Simultaneous enhancement of strength and ductility in ferrite-martensite steel via increasing the martensite fraction. *Mater. Chem. Phys.* **2021**, *259*, 124204. [CrossRef]
106. Deng, Y.-G.; Di, H.-S.; Misra, R.D.K. On significance of initial microstructure in governing mechanical behavior and fracture of dual-phase steels. *J. Iron Steel Res. Int.* **2018**, *25*, 932–942. [CrossRef]
107. Hao, X.; Zhao, X.; Huang, B.; Chen, H.; Ma, J.; Wang, C.; Yang, Y. Influence of Intercritical Quenching Temperature on Microstructure, Mechanical Properties and Corrosion Resistance of Dual-Phase Steel. *J. Mater. Eng. Perform.* **2020**, *29*, 4446–4456. [CrossRef]
108. Hashimoto, T. Fatigue life studies in carbon dual-phase steels. *Int. J. Fatigue* **1996**, *18*, 529–533. [CrossRef]

109. Nouri, A.; Saghafian, H.; Kheirandish, S. Effects of silicon content and intercritical annealing on manganese partitioning in dual phase steels. *J. Iron Steel Res. Int.* **2010**, *17*, 44–50. [CrossRef]
110. Sunil, B.; Rajanna, S. Evaluation of mechanical properties of ferrite-martensite DP steels produced through intermediate quenching technique. *SN Appl. Sci.* **2020**, *2*, 1461. [CrossRef]
111. Yaghoobi, F.; Jamaati, R.; Aval, H.J. A new 1.2 GPa-strength plain low carbon steel with high ductility obtained by SRDR of martensite and intercritical annealing. *Mater. Sci. Eng. A* **2020**, *788*, 139584. [CrossRef]
112. Nouri, A.; Kheirandish, S.; Saghafian, H. A Study of Redistribution of Silicon in Dual-Phase Silicon Steels. *Met. Sci. Heat Treat.* **2018**, *59*, 569–574. [CrossRef]
113. Davies, R.G. Influence of silicon and phosphorous on the mechanical properties of both ferrite and dual-phase steels. *Met. Mater. Trans. A* **1979**, *10*, 113–118. [CrossRef]
114. Pierman, A.-P.; Bouaziz, O.; Pardoen, T.; Jacques, P.; Brassart, L. The influence of microstructure and composition on the plastic behaviour of dual-phase steels. *Acta Mater.* **2014**, *73*, 298–311. [CrossRef]
115. Mohanty, R.R.; Girina, O.A.; Fonstein, N.M. Effect of Heating Rate on the Austenite Formation in Low-Carbon High-Strength Steels Annealed in the Intercritical Region. *Met. Mater. Trans. A* **2011**, *42*, 3680–3690. [CrossRef]
116. Kumar, R.; Patel, N.K.; Mukherjee, K.; Walunj, M.; Mandal, G.K.; Venugopalan, T. Ferrite channel effect on ductility and strain hardenability of ultra high strength dual phase steel. *Mater. Sci. Eng. A* **2017**, *685*, 187–193. [CrossRef]
117. Kim, N.J.; Thomas, G. Effects of morphology on the mechanical behavior of a dual phase Fe/2Si/0.1C steel. *Met. Mater. Trans. A* **1981**, *12*, 483–489. [CrossRef]
118. Paul, S.K.; Stanford, N.; Hilditch, T. Effect of martensite volume fraction on low cycle fatigue behaviour of dual phase steels: Experimental and microstructural investigation. *Mater. Sci. Eng. A* **2015**, *638*, 296–304. [CrossRef]
119. Moeini, G.; Ramazani, A.; Sundararaghavan, V.; Koenke, C. Micromechanical modeling of fatigue behavior of DP steels. *Mater. Sci. Eng. A* **2017**, *689*, 89–95. [CrossRef]
120. Idris, R.; Prawoto, Y. Influence of ferrite fraction within martensite matrix on fatigue crack propagation: An experimental verification with dual phase steel. *Mater. Sci. Eng. A* **2012**, *552*, 547–554. [CrossRef]
121. Ghosal, P.; Paul, S.K.; Das, B.; Chinara, M.; Arora, K.S. Notch fatigue performance of DP600 steel under different pre-straining paths. *Theor. Appl. Fract. Mech.* **2020**, *108*, 102630. [CrossRef]
122. Das, B.; Singh, A.; Arora, K.S.; Shome, M.; Paul, S.K. Influence of pre-straining path on high cycle fatigue performance of DP 600 steel. *Int. J. Fatigue* **2019**, *126*, 369–380. [CrossRef]
123. Lian, J.; Yang, H.; Vajragupta, N.; Münstermann, S.; Bleck, W. A method to quantitatively upscale the damage initiation of dual-phase steels under various stress states from microscale to macroscale. *Comput. Mater. Sci.* **2014**, *94*, 245–257. [CrossRef]
124. Rudnizki, J.; Prahl, U.; Bleck, W. Phase-field modelling of microstructure evolution during processing of cold-rolled dual phase steels. *Integr. Mater. Manuf. Innov.* **2012**, *1*, 19–31. [CrossRef]
125. Bleck, W.; Hömberg, D.; Prahl, U.; Suwanpinij, P.; Togobytska, N. Optimal Control of a Cooling Line for Production of Hot Rolled Dual Phase Steel. *Steel Res. Int.* **2014**, *85*, 1328–1333. [CrossRef]
126. Reséndiz-Flores, E.; Altamirano-Guerrero, G.; Costa, P.; Salas-Reyes, A.; Salinas-Rodríguez, A.; Goodwin, F. Optimal Design of Hot-Dip Galvanized DP Steels via Artificial Neural Networks and Multi-Objective Genetic Optimization. *Metals* **2021**, *11*, 578. [CrossRef]
127. Jolfaei, M.A.; Zhou, L.; Davis, C. Consideration of Magnetic Measurements for Characterisation of Ferrite–Martensite Commercial Dual-Phase (DP) Steel and Basis for Optimisation of the Operating Magnetic Field for Open Loop Deployable Sensors. *Metals* **2021**, *11*, 490. [CrossRef]
128. Liu, Y.; Fan, D.; Arróyave, R.; Srivastava, A. Microstructure-Based Modeling of the Effect of Inclusion on the Bendability of Advanced High Strength Dual-Phase Steels. *Metals* **2021**, *11*, 431. [CrossRef]
129. Rudomilova, D.; Prošek, T.; Traxler, I.; Faderl, J.; Luckeneder, G.; Schimo-Aichhorn, G.; Muhr, A. Critical Assessment of the Effect of Atmospheric Corrosion Induced Hydrogen on Mechanical Properties of Advanced High Strength Steel. *Metals* **2021**, *11*, 44. [CrossRef]
130. Alvarez, P.; Muñoz, F.; Celentano, D.; Artigas, A.; Cerda, F.M.C.; Ponthot, J.-P.; Monsalve, A. Modeling the Mechanical Response of a Dual-Phase Steel Based on Individual-Phase Tensile Properties. *Metals* **2020**, *10*, 1031. [CrossRef]
131. Drexler, A.; Bergmann, C.; Manke, G.; Kokotin, V.; Mraczek, K.; Pohl, M.; Ecker, W. On the local evaluation of the hydrogen susceptibility of cold-formed and heat treated advanced high strength steel (AHSS) sheets. *Mater. Sci. Eng. A* **2021**, *800*, 140276. [CrossRef]
132. Yaddanapudi, K.; Knezevic, M.; Mahajan, S.; Beyerlein, I.J. Plasticity and structure evolution of ferrite and martensite in DP 1180 during tension and cyclic bending under tension to large strains. *Mater. Sci. Eng. A* **2021**, *820*, 141536. [CrossRef]
133. Khosravani, A.; Caliendo, C.M.; Kalidindi, S.R. New Insights into the Microstructural Changes During the Processing of Dual-Phase Steels from Multiresolution Spherical Indentation Stress–Strain Protocols. *Metals* **2020**, *10*, 18. [CrossRef]
134. Costa, P.; Altamirano, G.; Salinas, A.; González-González, D.S.; Goodwin, F. Optimization of the Continuous Galvanizing Heat Treatment Process in Ultra-High Strength Dual Phase Steels Using a Multivariate Model. *Metals* **2019**, *9*, 703. [CrossRef]
135. Shen, X.; Tang, S.; Wang, G.; Zhang, Q.; Wang, X. Micro-laminated and ultrafine-grained dual-phase steel plates generated via intercritical rolling followed by water quenching. *J. Manuf. Process.* **2021**, *70*, 321–330. [CrossRef]

136. Xiong, Z.; Kostryzhev, A.G.; Zhao, Y.; Pereloma, E.V. Microstructure Evolution during the Production of Dual Phase and Transformation Induced Plasticity Steels Using Modified Strip Casting Simulated in The Laboratory. *Metals* **2019**, *9*, 449. [CrossRef]
137. Badkoobeh, F.; Mostaan, H.; Rafiei, M.; Bakhsheshi-Rad, H.R.; Berto, F. Friction Stir Welding/Processing of Mg-Based Alloys: A Critical Review on Advancements and Challenges. *Materials* **2021**, *14*, 6726. [CrossRef] [PubMed]
138. Xu, Y.; Dan, W.; Ren, C.; Huang, T.; Zhang, W. Study of the Mechanical Behavior of Dual-Phase Steel Based on Crystal Plasticity Modeling Considering Strain Partitioning. *Metals* **2018**, *8*, 782. [CrossRef]
139. Bräutigam–Matus, K.; Altamirano, G.; Salinas, A.; Flores, A.; Goodwin, F. Experimental Determination of Continuous Cooling Transformation (CCT) Diagrams for Dual-Phase Steels from the Intercritical Temperature Range. *Metals* **2018**, *8*, 674. [CrossRef]
140. Yang, Y.; Mi, Z.; Liu, S.; Li, H.; Li, J.; Jiang, H. The Impact of Strain Heterogeneity and Transformation of Metastable Austenite on Springback Behavior in Quenching and Partitioning Steel. *Metals* **2018**, *8*, 432. [CrossRef]
141. Liang, J.; Zhao, Z.; Wu, H.; Peng, C.; Sun, B.; Guo, B.; Liang, J.; Tang, D. Mechanical Behavior of Two Ferrite–Martensite Dual-Phase Steels over a Broad Range of Strain Rates. *Metals* **2018**, *8*, 236. [CrossRef]
142. Amigo, F.J.; Camacho, A.M. Reduction of Induced Central Damage in Cold Extrusion of Dual-Phase Steel DP800 Using Double-Pass Dies. *Metals* **2017**, *7*, 335. [CrossRef]
143. Evin, E.; Tomáš, M. The influence of laser welding on the mechanical properties of dual phase and trip steels. *Metals* **2017**, *7*, 239. [CrossRef]
144. Ji, F.; Song, W.; Ma, Y.; Li, C.; Bleck, W.; Wang, G. Recrystallization behavior in a low-density high-Mn high-Al austenitic steel undergone thin strip casting process. *Mater. Sci. Eng. A* **2018**, *733*, 87–97. [CrossRef]
145. Chang, Y.; Haase, C.; Szeliga, D.; Madej, L.; Hangen, U.; Pietrzyk, M.; Bleck, W. Compositional heterogeneity in multiphase steels: Characterization and influence on local properties. *Mater. Sci. Eng. A* **2021**, *827*, 142078. [CrossRef]
146. Haase, C.; Zehnder, C.; Ingendahl, T.; Bikar, A.; Tang, F.; Hallstedt, B.; Hu, W.; Bleck, W.; Molodov, D.A. On the deformation behavior of κ-carbide-free and κ-carbide-containing high-Mn light-weight steel. *Acta Mater.* **2017**, *122*, 332–343. [CrossRef]
147. Naalchian, M.; Kasiri-Asgarani, M.; Shamanian, M.; Bakhtiari, R.; Bakhsheshi-Rad, H.R.; Berto, F.; Das, O. Phase Formation during heating of amorphous nickel-based BNi-3 for joining of dissimilar cobalt-based superalloys. *Materials* **2021**, *14*, 4600. [CrossRef] [PubMed]
148. Naalchian, M.; Kasiri-Asgarani, M.; Shamanian, M.; Bakhtiari, R.; Bakhsheshi-Rad, H.R. Effect of Substrate's Heat Treatment on Microstructure and Mechanical Properties TLP Bonding of Dissimilar X-45/FSX-414 Cobalt Based Superalloys. *Met. Mater. Int.* **2021**, *27*, 4657–4668. [CrossRef]
149. Abazari, S.; Shamsipur, A.; Bakhsheshi-Rad, H.R.; Ismail, A.F.; Sharif, S.; Razzaghi, M.; Ramakrishna, S.; Berto, F. Carbon nanotubes (CNTs)-reinforced magnesium-based matrix composites: A comprehensive review. *Materials* **2020**, *13*, 4421. [CrossRef]
150. Abazari, S.; Shamsipur, A.; Bakhsheshi-Rad, H.R.; Ramakrishna, S.; Berto, F. Graphene family nanomaterial reinforced magnesium-based matrix composites for biomedical application: A comprehensive review. *Metals* **2020**, *10*, 1002. [CrossRef]
151. Mudang, M.; Hamzah, E.; Bakhsheshi-Rad, H.R.; Berto, F. Effect of heat treatment on microstructure and creep behavior of Fe-40Ni-24Cr alloy. *Appl. Sci.* **2021**, *11*, 7951. [CrossRef]
152. Ma, Y.; Sun, B.; Schökel, A.; Song, W.; Ponge, D.; Raabe, D.; Bleck, W. Phase boundary segregation-induced strengthening and discontinuous yielding in ultrafine-grained duplex medium-Mn steels. *Acta Mater.* **2020**, *200*, 389–403. [CrossRef]